Snapshots of pre-glacial paleoenvironmental conditions along the Sabrina Coast, East Antarctica: New palynological and biomarker evidence

Meghan Duffy, Emily Tibbett, Catherine Smith, Sophie Warny, Sarah Feakins, Gilles Escarguel, Rosemary Askin, Amy Leventer, Amelia Shevenell

Snapshots of pre-glacial paleoenvironmental conditions along the Sabrina Coast, East Antarctica: new palynological and biomarker evidence ✡

Meghan Duffy [a,*], Emily J. Tibbett [b], Catherine Smith [c], Sophie Warny [a], Sarah J. Feakins [b], Gilles Escarguel [d], Rosemary Askin [e], Amy Leventer [f], Amelia E. Shevenell [g]

[a] Department of Geology and Geophysics and Museum of Natural Science, Louisiana State University, Baton Rouge, LA, USA

[b] Department of Earth Sciences, University of Southern California, Los Angeles, CA, USA

[c] International Ocean Discovery Program, Texas A&M University, College Station, TX, USA

[d] Univ Lyon, Université Claude Bernard Lyon 1, CNRS, ENTPE, UMR 5023 LEHNA, 69622 Villeurbanne, France

[e] Consultant, Jackson, Wyoming, USA

[f] Department of Geology, Colgate University, Hamilton, NY, USA

[g] College of Marine Science, University of South Florida, St. Petersburg, FL, USA

* Corresponding author. Email address: mduffy7@lsu.edu (M. Duffy).

✡ Corresponding editor: Séverine Fauquette.

Abstract

The Aurora Subglacial Basin (ASB) catchment contains 3-5 m of sea-level equivalent ice volume that drains to the Sabrina Coast, East Antarctica via the Totten Glacier system. Observed thinning and retreat of Totten Glacier indicate regional sensitivity to oceanographic and atmospheric warming. Paleoclimate studies of climatically sensitive catchments are required to understand the evolution of the East Antarctic Ice Sheet (EAIS) and its outlet

glacier systems. Recent seismic and sediment studies from the Sabrina Coast document the evolution of the EAIS in the ASB catchment, suggesting that the region has long been sensitive to climatic changes. This study presents new palynological and biomarker data from Sabrina Coast continental shelf sediments. Detailed palynological records were obtained from four short jumbo piston cores (JPC; NBP14-02 JPC-30, -31, -54 and -55), enabling reconstructions of regional vegetation and environments prior to and during Cenozoic EAIS development. The Sabrina Flora is dominated by angiosperms, with *Gambierina* spp. often exceeding 40% of the assemblage, and diverse Proteaceae, *Battenipollis* spp., *Forcipites* spp., *Nothofagidites* spp., fern, and conifer palynomorphs indicative of an open shrubby ecosystem. Excellent preservation and frequent occurrence of *Gambierina* spp. clusters suggest that a majority of the Sabrina Flora assemblage is penecontemporaneous with sedimentation; however, some uncertainties remain whether this sedimentation occurred in the Late Cretaceous or the Paleogene. Despite that uncertainty, high abundances of *Gambierina* spp. and *Battenipollis* spp., in combination with relatively low (<10%) *Nothofagidites* spp. abundances indicate that the Sabrina Flora is unique in Antarctica. Evaluation of biomarkers finds evidence for penecontemporaneous and reworked components. The penecontemporaneous C_{30} *n*-alkanoic acids have $\delta^{13}C$ values of -30.2 ± 0.5‰, consistent with $\delta^{13}C$ values in an open canopy woodland or shrubby open vegetation. Their hydrogen isotope (δD) values of -215 ± 4.5‰, indicate precipitation isotopic composition (δD_{precip}) of -130‰, similar to coastal snow in the same region today. Together, Sabrina Flora palynomorph and plant wax data suggest a drier, more open coastal vegetation in the Aurora Basin of East Antarctica rather than the closed rainforest vegetation often described from other parts of Antarctica for the Cretaceous to Paleogene. To directly compare records from the circum-Antarctic, additional long sedimentary records with improved biostratigraphic constraints are required. Such records will enable identification of regional climate gradients or micro-climates, and allow assessment of the environmental conditions and mechanisms driving observed differences.

Keywords:
East Antarctica
Paleogene
Cretaceous
Palynology
Paleovegetation

1. Introduction

The East Antarctic Ice Sheet (EAIS), which contains 53 m of sea level equivalent ice, is one of the largest potential contributors to modern sea level rise (Fretwell et al., 2013; DeConto and Pollard, 2016; Morlinghem et al., 2020). The Aurora Subglacial Basin (ASB) (Fig. 1) contains 3.9 m of sea level equivalent ice that is drained by the Totten Glacier and its tributaries that terminate at the Sabrina Coast, East Antarctica (Young et al., 2011; Wright et al., 2012; Greenbaum et al., 2015, Morlinghem et al., 2020). The Sabrina Coast (115° to 121°E, 67°S) is located on the Wilkes Land continental margin (Young et al., 2011), which formed as Antarctica rifted from Australia in the mid-Cretaceous (Cande and Mutter, 1982; Escutia et al., 2011). As a major drainage outlet of the ASB, sediments deposited on the Sabrina Coast shelf likely contain historical records of glacial evolution in the ASB (Gulick, Shevenell et al., 2017; Montelli et al., 2019).

Geologic and oxygen isotope data from deep-sea benthic foraminifera indicate continental-scale ice sheets were present in East Antarctica by at least the early Oligocene (Kennett, 1977; Coxall et al., 2005; Francis et al., 2009); however, the history of the EAIS prior to this time remains poorly understood. Recent airborne and marine geophysical and geological studies of the ASB and the sediments from the Sabrina Coast continental shelf document the Cenozoic evolution of the EAIS in the ASB, revealing that regional outlet glaciers expanded progressively seaward and became marine terminating as early as the middle Eocene (Young et al., 2011; Wright et al., 2012; Aitken et al., 2016; Gulick, Shevenell et al., 2017; Montelli et al., 2019). Large volumes of sediment eroded from the ASB were transported to the Sabrina Coast by glacio-fluvial systems, resulting in continental shelf progradation in the early Paleogene (Gulick, Shevenell et al., 2017). Paired marine seismic and sedimentologic studies of short jumbo piston cores from the Sabrina Coast shelf indicate that regional glaciers advanced and retreated across the shelf at least 11 times in the Oligocene and Miocene, suggesting the EAIS was not as stable as previously thought (Gulick, Shevenell et al., 2017; Montelli et al., 2019).

Here we present new pollen assemblage and biomarker records from short sediment cores recovered from the Sabrina Coast shelf that provide insights into the Late Cretaceous to Paleogene paleoclimate and vegetation history of the ASB catchment. Our data increase the resolution of previously published palynological records (Gulick, Shevenell et al. 2017; Smith et al., 2019). We also add new biomarker data that suggest an environmental significance for

several palynomorphs with unknown botanical affinities and provide insight to past East Antarctic climate. Additionally, late Miocene to early Pliocene sediments provide insight to sedimentary reworking processes along the Sabrina Coast.

2. Material and methods

2.1. Material

This study is based upon four short (<2 m) jumbo piston cores (JPC-30, -31, -54, and -55 from cruise NBP14-02; Gulick, Shevenell et al., 2017; Fig. 2). Seismic imaging of the Sabrina Coast continental shelf identified three distinct sedimentary packages, termed Megasequences I-III (MS-I, MS-II, and MS-III; Gulick, Shevenell et al., 2017). MS-I, which overlies basement, contains 620 m of seaward-dipping, low-amplitude discontinuous reflectors with at least two clinoforms indicating periods of high sediment flux. An undulating eroded surface separates MS-I from MS-II and is interpreted to reflect evidence for the first grounded ice on the continental shelf (Gulick, Shevenell et al., 2017; Montelli et al., 2019). MS-II is 675 m thick and contains at least 11 erosive surfaces within a sequence of laminated to acoustically transparent sediments indicative of ice proximal to open marine sediments (Gulick, Shevenell et al., 2017; Montelli et al., 2019). These erosive surfaces indicate a minimum of 11 glacial advances and retreats across the middle shelf during the deposition of MS-II (Gulick, Shevenell et al., 2017; Montelli et al., 2019). A regional unconformity separates MS-II from MS-III, with evidence of significant glacial erosion into MS-II. Glacial erosion of the seafloor allowed Gulick, Shevenell et al. (2017) to sample exposed sediment from MS-I (NBP14-02 JPC-54 and -55) and through the regional unconformity (NBP14-02 JPC-30 and -31).

As described by Gulick, Shevenell et al. (2017), JPC-54 (66.28°S, 120.67°E; water depth: 442 m) and JPC-55 (66.35°S, 120.51°E; water depth: 520 m) are 121 cm and 169 cm in length, respectively (Figs. 2, 3). Core sites were chosen based on high-resolution seismic data from NBP14-02 seismic line 17, which revealed pre-glacial strata outcropping at the seafloor. JPC-54 and JPC-55 were collected from MS-I, above and below a clinoform, respectively. Each core consists of two units separated by a sharp contact. In both cores, Unit I (20 cm in JPC-54 and 40 cm in JPC-55) consists of late Quaternary diatom-rich mud, which overlies a partially consolidated sandy interval (Unit II). In JPC-54, Unit II (101 cm) consists of structureless diamict to silty coarse sands with centimeter-scale angular lonestones, while in JPC-55 Unit II (129 cm) consists of more consolidated black micaceous

silty sands with organic detritus, macro- and microfossils, and rare pyrite nodules (Gulick, Shevenell et al., 2017). Core lithologies are shown in Fig. 3.

Thirteen samples collected from JPC-54 and JPC-55 for preliminary palynological analysis (Gulick, Shevenell, et al., 2017; Smith et al., 2019) contributed biostratigraphic information used in conjunction with foraminiferal samples to provide initial age-control for the Unit II sediments in each jumbo piston core. Smith et al. (2019) documented an unexpectedly abundant, diverse, and well-preserved terrestrial palynomorph assemblage, named the Sabrina Flora. This flora, dominated by two new pollen species, has the potential to contribute to limited existing knowledge of the paleobotanical history of East Antarctica. Preliminary analysis showed that the Sabrina Flora is dominated by angiosperms, with *Gambierina (G.) rudata* and *G. edwardsii* complexes often exceeding 40% of the assemblage (Smith et al., 2019). Additionally, diverse Proteaceae, *Battenipollis sectilis*, *Forcipites* spp., *Nothofagidites (N.)* spp., fern and conifer palynomorphs contribute to the assemblage. Smith et al. (2019) also described two new species: *Battenipollis sabrinae* and *Gambierina askiniae*. Pristine pollen preservation, the frequent occurrence of *Gambierina* spp. clusters, and the geomorphology of the ASB and Sabrina shelf, led Smith et al. (2019) to interpret a majority of the *Sabrina Flora* assemblage as penecontemporaneous with sedimentation.

2.2. Age control: a review of uncertainties and hard facts

2.2.1. NBP14-02 JPC-54 and -55

To constrain the age of Unit II in each short sediment core collected from the Sabrina Shelf, Gulick, Shevenell et al. (2017) and Smith et al. (2019) used published age ranges of pollen when available and data on foraminifer species observed in NBP14-02 JPC-54 and -55. Due to the paucity of palynostratigraphic data from the East Antarctic margin, they incorporated age constraints from a limited number of key species from southern Australian and New Zealand (e.g., Stover and Partridge, 1973; Jarzen and Dettmann, 1992; Partridge, 2006), the Antarctic Peninsula (e.g., Francis et al., 2009; Warny and Askin, 2011; Warny et al., 2019), and McMurdo Sound erratics (e.g., Askin, 2000; Francis, 2000; Levy and Harwood, 2000). A detailed discussion of the methods used to establish preliminary age control in JPC-54 Unit II and JPC-55 Unit II can be found in Gulick, Shevenell et al. (2017) and Smith et al. (2019). In these publications, JPC-54 was determined to have an age of early to middle Eocene, based on pollen biostratigraphy, while JPC-55 was determined to be of latest Paleocene age, based on a combination of pollen and foraminiferal biostratigraphy. The presence of benthic foraminifera in JPC-55 indicate that sediment was deposited in a marine

shelf environment and pollen clusters suggest that the terrestrial-derived sedimentary component was not likely transported over significant distances or substantially reworked (Gulick, Shevenell, et al., 2017; Smith et al., 2019). The overlap in foraminifer species ranges indicates a Paleocene age for JPC-55 Unit II (Gulick, Shevenell et al., 2017). The Paleocene age of JPC-55 was further refined to late Paleocene using the presence of *Microalatidites paleogenicus*, which has a first Antarctic occurrence in the early Paleocene (Truswell and Macphail, 2009; Raine et al., 2011) and the first occurrences of *Nothofagidites lachlaniae*, *Proteacidites tenuiexinus*, and *N. flemingii-rocaensis* complex in the late Paleocene (Stover et al., 1973; Stover and Evans, 1973).

Recently an alternative interpretation of the Sabrina Flora (Macphail, 2021) suggested a Late Cretaceous age, based on comparison to pollen from the Great Australian Bight sub-basins (Dettmann et al., 1990; Partridge, 1999). Macphail (2021) also cited unpublished evidence for abundant pollen identical to *Battenipollis sabrinae* and *Gambierina askiniae* in Campanian to Maastrichtian sediments recovered from the Gippsland Basin, Australia, and reinterpreted the Sabrina Flora of Smith et al. (2019) to be also Late Cretaceous in age. While we acknowledge the possibility that the Sabrina Flora is of Late Cretaceous age and reworked (Macphail, 2021), we argue that it is more plausible that Unit II in JPC-55 is of Paleocene age, when considering the totality of the published pollen and foraminifer data, the seismic facies, and the stratigraphic context of the Sabrina shelf sedimentary sequence (Gulick, Shevenell et al., 2017; Smith et al., 2019; Montelli et al., 2020). Further, because JPC-54 was recovered ~30 m above JPC-55, stratigraphically, we can state with high confidence that JPC-54 sediments are younger than those in JPC-55, but older than the unconformity interpreted to reflect the first expansion of glacial ice across the Sabrina Coast shelf (Gulick, Shevenell et al., 2017; Smith et al., 2019; Montelli et al., 2020).

This said, because the two studied sequences are <2 m in length and the extent of reworking cannot definitively be assessed, we will not exclude the Late Cretaceous as a possible source of the floral organic matter recovered. But until longer sedimentary sequences are drilled on the Sabrina Coast shelf, we accept the published Paleocene age for JPC-55 and the larger early to middle Eocene age range for JPC-54 (Gulick, Shevenell et al., 2017; Smith et al., 2019).

2.2.2. NBP14-02 JPC-30 and -31

To assess sedimentary reworking in Sabrina Coast sediments, we analyzed cores JPC-30 (66.45°S, 120.33°E; water depth: 548 m) and JPC-31 (66.45°S, 120.34°E, water depth:

534 m), which recovered the MS-II/MS-III contact and are late Miocene to early Pliocene in age, as indicated by well-defined diatom biostratigraphy (Gulick, Shevenell et al., 2017; Figs. 2, 3). As such, MS-II erosive surfaces, interpreted to reflect glacial advances and retreats, were likely formed during the Oligocene and Miocene (Gulick, Shevenell et al., 2017). Current knowledge of Antarctic plant evolution indicates that vegetation essentially disappeared from the Antarctic Peninsula at 12.8 Ma (Anderson et al., 2011) and from the Dry Valleys at ca. 13.85 Ma (Lewis et al., 2008; Rau, 2017). In the ASB, it is likely that palynomorph production ceased following the large-scale glaciation evidenced by the regional unconformity observed in the Sabrina Coast seismic profiles (Gulick, Shevenell et al., 2017). We suggest that all palynomorphs observed in JPC-30 and -31 are reworked and do not provide biostratigraphic information. However, analysis of reworked palynomorphs is useful in understanding sediment transport to the Sabrina Coast and provides insight to the type of sediments eroded by ice advance (e.g., Baudoin, 2018; Coenen et al., 2019).

2.3. Palynology

To quantify absolute abundance of terrestrial palynomorphs and discern palynomorph assemblages from JPC-30, -31, -54 and -55, six samples from JPC-30, five samples from JPC-31, 23 samples from JPC-54 and 34 samples from JPC-55 (Fig. 3) were collected and processed for terrestrial palynomorphs at Global Geolab Limited (Alberta, Canada). For each sample preparation, ~5 g of dried sediment was spiked with a known quantity of *Lycopodium* spores to allow for the quantitative assessment of terrestrial palynomorph concentrations. Acid soluble minerals (carbonates and silicates) were digested in HCl and HF, followed by a controlled oxidation of the residue. Rinsing to neutrality with DI water was performed between each steps. Residues were concentrated by filtration on a 10 μm mesh sieve.

The 68 samples from JPC-30, -31, -54, and -55 were examined using an Olympus BX41 microscope with ×60 and ×100 oil immersion lenses. A minimum of 300 terrestrial palynomorphs were counted per sample, using a snaking transect method. In low abundance samples, the entire slide was counted; *Lycopodium* spores were also counted. A database of all palynomorphs recovered was prepared and key species documented photographically using a Q-Color 5 Olympus camera system with Q-Capture (v. 3.1.1) software. Taxonomic evaluation of palynomorphs utilized established literature (e.g., Cookson, 1950; Cookson and Pike, 1954; Couper, 1960; Stover and Partridge, 1973; Truswell, 1983; Jarzen and Dettmann, 1992; Macphail and Truswell, 2004; Hou et al., 2006; Truswell and Macphail, 2009; Raine et al., 2011; Pross et al., 2012; Contreras et al., 2013; Smith et al., 2019) and collections curated

at the Louisiana State University Center for Excellence in Palynology (CENEX). Shannon Diversity Index (H) was calculated as $H = -\sum p_i \cdot ln(p_i)$, where p_i is the proportion of individuals belonging to the i^{th} species in the dataset.

2.4. Biomarkers

Eleven samples from JPC-54 and -55 were freeze-dried and 4-21 g of sediment was homogenized for extraction via an Accelerated Solvent Extraction (ASE 350, Dionex) using a 9:1 Dichloromethane (DCM) to methanol (MeOH) mixture (v/v). Resulting total lipid extracts were separated into neutral and acid fractions via column chromatography through LC-NH_2 gel (columns were 5 cm × 40 mm Pasteur pipette with NH_2 sepra bulk packing) using 2:1 DCM:isopropanol and 4% formic acid in diethyl ether to separate out the neutral and acid fractions, respectively. The neutral fraction was separated via column chromatography using 5% deactivated silica gel, eluting the *n*-alkanes in the hexane fraction, and the polar biomarkers with DCM and MeOH. The acid fraction, containing the *n*-alkanoic acids, were methylated using 95% MeOH of a known isotopic composition with 5% hydrochloric acid for 12 hours at 70°C. The fatty acid methyl esters (FAMEs) were separated using 2:1 hexane:MilliQ water (v/v) and dried by passing through anhydrous sodium sulfate, and further purified over silica gel column chromatography eluting first with hexane to exclude any further impurities and then with DCM to recover the FAMEs. Both *n*-alkanes and FAMEs fractions were analyzed by gas chromatography mass spectrometry (GC-MS) for compound identification and the *n*-alkanes and *n*-alkanoic acids as methyl esters were quantified via Flame Ionization Detection, in comparison to in-house alkanes and FAME standards, respectively. We quantified the abundance of individual *n*-alkanes and *n*-alkanoic acids and calculated the average chain length (ACL) and carbon preference index (CPI) as follows:

$$\mathrm{ACL} = \frac{\sum(n * [C_n])}{\sum [C_n]}$$

$$\mathrm{CPI} = \frac{\sum C_n}{\sum C_{n-1}}$$

where *n* = 24-30 for *n*-alkanoic acids and 23-31 for the *n*-alkanes. The CPI is calculated as the even over odd preference for *n*-alkanoic acids, the odd over even preference for alkanes, and the even over odd preference for *n*-alkanes. Within the alkanes fraction, we measured the relative abundances of hopanes, biomarkers that derive from membrane lipids in bacteria and that undergo isomerization with increasing thermal maturity (Inglis et al., 2020). We

identified these compounds using their diagnostic mass fragments and comparison to published spectra (Inglis et al., 2018; Sessions et al., 2013; Uemura and Ishiwatari, 1995).

Compound specific isotope analysis was performed on the FAMEs fraction using a gas chromatography isotopic ratio mass spectrometer (GC-IRMS) using a Thermo Scientific Trace gas chromatograph connected to a Delta V Plus mass spectrometer via an Isolink combustion furnace at 1000°C for $\delta^{13}C$ and a pyrolysis furnace at 1400°C for δD. The peak amplitude was 1-7 V. The $\delta^{13}C$ linearity was recorded each day and had an average standard deviation of 0.042‰. H_3 factor was recorded every day with an average value of 9.518 ± 0.377 ppm mV^{-1}. Samples were normalized to Vienna Pee Dee Belemnite (VPDB) and Vienna Standard Mean Ocean Water/Standard Light Antarctic Precipitation (VSMOW/SLAP) by an external standard mixture of 16 *n*-alkanes with $\delta^{13}C$ values that range from -25.9 to -33.7‰ and δD values from -17 to -256‰ (A6 mix obtained from A. Schimmelmann, Indiana University). Corrections were made for the methyl group added during methylation for the *n*-alkanoic acids ($\delta^{13}C$ of -24.7 ± 0.2‰ and δD of -186.9 ± 3.7‰) by mass balance to calculate the isotopic composition of the corresponding acid.

2.5. Statistical analysis

Statistical analyses on palynomorph abundance and assemblage data were conducted using PAST v. 2.17c freeware (Hammer et al., 2001). Stratigraphically-unconstrained and stratigraphically-constrained analyses using the Bray-Curtis similarity index and Correspondence Analysis (Legendre and Legendre, 2012) were used to examine changes in palynomorph assemblages between and among the four cores. Analysis of Similarity (ANOSIM; Clarke, 1993) also based on the Bray–Curtis similarity matrix was done to identify sample clusters with different taxonomical compositions, followed by Similarity Percentage analysis (SIMPER; Clarke, 1993) in order to determine which taxa control the significant differences among clusters.

3. Results

3.1. Palynology

The samples from NBP14-02 JPC-54 and -55 (Unit II) reveal a Sabrina Flora with abundant, well-preserved palynomorphs in high abundances that range from ~5,000 to 19,000 palynomorphs per gram of dried sediment, with a minimum of 62 species present. The assemblages are dominated by angiosperms, with *Gambierina* (*G.*) spp. often exceeding 40% of the assemblage. Diverse Proteaceae, *Battenipollis* (*B.*) spp., *Forcipites* spp., *Nothofagidites*

spp., fern and conifer palynomorphs are also notable in the JPC-54 and -55 assemblages. Clusters of *Gambierina* spp., *Battenipollis* spp., *Proteacidites* spp., *Forcipites* sp., and *Nothofagidites* sp. are also observed throughout Unit II in both JPC-54 and -55. Low abundances of darker, reworked Cretaceous and Permian palynomorphs are observed, including *Cicatricosisporites ludbrooki*, *Granulatisporites* sp., and *Leiotriletes directus*.

A UPGMA cluster analysis on a Bray-Curtis similarity matrix with no stratigraphic constraint identified four statistically significant clusters (G1, G2, G3, G4) in the complete dataset from all four cores (Fig. 4):

- cluster G1 includes all samples from JPC-30 and -31;
- cluster G2 includes all JPC-54 Unit II samples;
- cluster G3 includes all Unit I samples from JPC-55 and one sample from JPC-54;
- cluster G4 includes all JPC-55 Unit II samples;
- the two uppermost (Unit I) samples from JPC-54 do not fall within a statistically significant group.

Eighteen of 62 identified taxa explain >80% of the overall compositional differences between the four clusters; all other taxa individually explain <1.2% and together explain <20% of the overall compositional differences between the clusters (Table 1).

In core NBP14-02 JPC-55, palynomorph abundance averages 362 (Unit I) and 10,212 (Unit II) palynomorphs per gram of dried sediment. Diversity in Unit I is low (H = 1.7) and significantly higher in Unit II (H = 2.8; Fig. 5). For all JPC-55 samples, a stratigraphically-constrained UPGMA cluster analysis on a Bray-Curtis similarity matrix reveals three distinct groups (55-1, 55-2, and 55-3) which are statistically different from one another (Fig. 6). Group 55-1 contains all samples from Unit I, where the assemblage is dominated by *G. rudata,* with *B. sectilis* subdominant. The sample at 49 cm depth, close to the contact between Units I and II, did not fall in any of the three groups. Groups 55-2 and 55-3 contain all other samples from lithologic Unit II. In this unit, *G. askinae* and *B. sabrinae* are co-dominant, with notable contributions from *Proteacidites* spp. (especially *P. parvus*), *Forcipites* spp., *B. sectilis*, *Nothofagidites* spp., and gymnosperm pollen, including *Podocarpidites* spp.

In core NBP14-02 JPC-54, palynomorph abundance averages 441 (Unit I) and 8,287 (Unit II) palynomorphs per gram of dried sediment. As in JPC-55, JPC-54 Unit I diversity is low (H = 1.8) and is significantly greater in Unit II (H = 2.8) (Fig. 7). For all JPC-54 samples, a stratigraphically-constrained UPGMA cluster analysis on a Bray-Curtis similarity matrix reveals three groups (54-1, 54-2, and 54-3). Group 54-1 is statistically distinct from groups

54-2 and 54-3 but groups 54-2 and 54-3 are not statistically different from each other (Fig. 8). Samples from 17 cm (close to the Unit I/II boundary) and 68 cm depth did not fit into any of the three groups. Group 54-1 contains samples from lithologic Unit I, whose assemblage is dominated by *G. rudata,* with *B. sectilis* subdominant. Groups 54-2 and 54-3 contain samples from lithologic Unit II, where *G. rudata* is dominant, with notable contributions from *Nothofagidites* spp. (especially *N. lachlaniae)*, *Proteacidites* spp., *B. sectilis*, *Forcipites* spp., and gymnosperm pollen including *Podocarpidites* spp.

The cores NBP14-02 JPC-30 and -31 both contain low abundances of palynomorphs, with concentrations averaging 49 and 44 palynomorphs per gram of dried sediment, respectively (Figs. 9, 10). The palynomorph assemblages are somewhat low in diversity (H = 2.2 and 2.3, respectively) and are statistically indistinguishable from one another (Fig. 4), with *G. rudata* dominant, and *Cyathidites minor* and *B. sectilis* sub-dominant.

Because the significant compositional differences between groups in all four sediment cores were driven by 18 main taxa (Table 1), a Correspondence Analysis was performed on only those taxa. This analysis shows groups G1, 55-1 and 54-1 clearly separated from 55-2, 55-3, 54-2, and 54-3 (Fig. 11). The resulting factorial space (two first factorial axes) shows the driving taxa of this sample distribution along each factorial axis (Fig. 12). Factorial Axis 1 (50.7% of the overall between-sample variation) is driven by changes in abundance of *B. sabrinae* and *G. askinae* vs. *B. sectilis* and *G. rudata.* Groups G1, 54-1 and 55-1 are characterized by high abundances of *B. sectilis* and *G. rudata* relative to *B. sabrinae* and *G. askinae*. Groups 54-2 and 54-3 are characterized by moderate to low relative abundances of *B. sectilis* and *G. rudata*. Groups 55-2 and 55-3 are characterized by very low relative abundances of *B. sectilis* and *G. rudata* relative to *B. sabrinae* and *G. askinae*. Factorial Axis 2 (21.7% of the overall between-sample variation) is driven by changes in abundance of *B. sectilis*, *Forcipites stipulatus* and *Proteacidites parvus* vs. *Laevigatosporites ovatus*, *N. lachlaniae*, *Liliacidites* spp., *Proteacidites* spp., *Arecipites* spp., and trilete cryptogam spores.

3.2. Biomarkers

Both *n*-alkane and *n*-alkanoic acid fractions were evaluated in Unit II of cores JPC-54 and JPC-55. All samples contained *n*-alkanes and hopanes, except for in sample JPC-55-147 cm, where concentrations were below detection limits. We identified C_{17} to C_{31} *n*-alkanes above an uncharacterized complex mixture (UCM) in all samples. The concentration of detected (C_{17} to C_{31}) *n*-alkanes ranged from 128 to 440 ng/gdw with long chain *n*-alkanes, likely derived from plants (C_{23}-C_{31}), ranging between 71 to 265 ng/gdw (Fig. 13(B)). ACL

was in the range of 26 to 27 (Fig. 13(C)). The CPI was low, averaging 2.2 and 1.8 for JPC-54 and -55, respectively (Fig. 13(D)), consistent with evidence for maturity from the UCM. Within the alkanes fraction, we also identified C_{27} to C_{31} hopanes and their isomers. We report the hopane index ββ/(αβ+βα+ββ) for the available isomers of C_{29} hopanes only, C_{31} hopanes only, and due to variations in the ability to detect C_{29} and C_{31} stereoisomers across the two cores, we computed the index across all available C_{27} to C_{31} hopane isomers (Fig. 13(A)), similar to Duncan et al. (2019). Applying the hopane index across all long chain hopanoids yields average values of 0.62 and 0.41 for JPC-54 and -55, respectively, suggesting generally low to moderate thermal maturity; a single low value (0.06) at 52 cm in JPC-55 suggests the presence of high thermal maturity carbon. However, variability between samples suggests variable inputs of reworked components.

The *n*-alkanoic acids were more abundant than the *n*-alkanes. We found C_{16} to C_{30} *n*-alkanoic acid homologues with an even over odd chain length distribution, indicating penecontemporary inputs, with the shorter chains likely from aquatic production and the longer chain homologues most likely to be exclusively derived from plant wax. The long chain *n*-alkanoic acids (C_{24}-C_{30}) had concentrations ranging from 313 to 3,330 ng/gdw (Fig. 13(B)) with an average concentration of 1,929 ng/gdw and 542 ng/gdw for JPC-54 and -55, respectively. The C_{30} *n*-alkanoic acids are present with concentrations ranging from 78 to 1,172 ng/gdw. The ACL averaged 26.4 and 26.2 (Fig. 13(C)), with a CPI average of 8.2 and 4.9 for JPC-54 and -55, respectively (Fig. 13(D)); these distributions are indicative of penecontemporary plant wax inputs. Given their abundance and penecontemporary interpretation, the *n*-alkanoic acids were analyzed for compound specific carbon and hydrogen isotopic compositions.

In cores JPC-54 and -55, the $\delta^{13}C$ values for the C_{24}, C_{26} and C_{28} *n*-alkanoic acids range from -29 to -25‰, which suggests a shifting proportion of marine or microbial sources across the homologous series. C_{30} and C_{32} have similar $\delta^{13}C$ values, which are offset from C_{24}, C_{26} and C_{28} *n*-alkanoic acid $\delta^{13}C$ values, supporting the use of C_{30} and C_{32} as terrestrial plant biomarkers (Fig. 13(F)). The longer chain C_{30} and C_{32} *n*-alkanoic acid compounds are thus suitable for reconstructions of the hydrogen isotopic composition of precipitation as recorded by terrestrial plants. Downcore $\delta^{13}C_{30}$ values in JPC-54 range from –31.2 to –29.9‰ with an average value of –30.2 ± 0.5‰ (Fig. 13). The $\delta^{13}C_{30}$ was not measured in JPC-55 due to low $C_{30\text{-acid}}$ abundance and prioritization of hydrogen isotopic analyses.

The C_{30} *n*-alkanoic acid has a mean δD value of –216 ± 5‰, and ranges between –222 and –207‰ across both JPC-54 and -55 (Fig. 13(E)). A net fractionation of –100‰ was the

approximation used for open vegetation environments in other Antarctic margin settings (Feakins et al., 2012, 2014). More recently a suite of studies of *n*-alkanoic acids in high latitude boreal ecosystems suggested fractionations for the C_{28} *n*-alkanoic acid in Siberia of –107 ± 12‰ (Wilkie et al., 2013) and –95 ± 11‰ in the boreal forest ecosystems of the Yukon, Alaska and Northwest Territories (Bakkelund et al., 2018). Greenland surveys suggest consistency of high latitude plants net fractionations with a global mean estimate of –99‰ (McFarlin et al., 2019), hence all estimates are equivalent within uncertainties. Given the lack of calibration of austral high latitude ecosystems, uncertainty in the appropriate value is unavoidable and unknown. Therefore, we use the approximate net fractionation of –100‰, for comparability with prior Antarctic paleoclimate reconstructions and consistent with the boreal calibration ranges. Uncertainty in the net fractionation is estimated to be on the order of 10‰ based on boreal calibrations. This indicates δD_{precip} values range from –136 to –118‰, with a mean δD_{precip} of –129 ± 6‰ across both JPC-54 and -55.

4. Discussion

4.1. Palynomorph and biomarker provenance and regional hydroclimate

Seismic data and benthic foraminifers indicate that siliciclastic sediments with terrestrial organic debris recovered in JPC-55 were deposited in a proximal marine shelf setting seaward of a low-lying fluvial and/or glaciofluvial environment (Young et al., 2011; Wright et al., 2012; Aitken et al., 2016; Gulick, Shevenell et al., 2017; Montelli et al., 2020). Although longer records are required to definitively assess reworking, we suggest that a majority of the Sabrina Flora assemblage was likely locally sourced from the low-lying coastal plain and delivered to the shelf via low-energy fluvial outflow during time intervals of relatively high sea level (e.g., the late Paleocene). Support for this interpretation comes from the following lines of evidence:

- pristine preservation of palynomorphs in Unit II sediments in both JPC-54 and -55, which indicates an assemblage that has not been vigorously reworked;
- values obtained for the hopane index across all long chain hopanoids and the light color of the grains, both indicating low thermal maturity in contrast to the species that we know are definitely reworked from Permian and Lower Cretaceous sediments;
- the high concentration in pollen recovered in Unit II as opposed to concentrations recovered from Unit I and cores JPC-30 and -31;

- the frequent occurrence of angiosperm palynomorph clusters that suggests deposition close to the parent plant, with little opportunity for dispersion of individual grains (Smith et al., 2019).

However, fluvial/glaciofluvial processes leave open the possibility of selective erosion and deposition of older reworked terrestrial sediments sourced from the central Aurora and Sabrina Basins (Young et al., 2011; Aitken, 2016).

Plant derived biomarkers from Sabrina Coast shelf sediments provide further information on both transport history and paleoenvironment. Plant wax δD values are relatively stable across both JPC-54 and -55, a stability which is remarkable given their difference in age. Paleoprecipitation estimates indicate a δD_{precip} ranging from –136 to –118‰, with a mean of –129 ± 6‰, slightly more positive than coastal snow in the same region today (–133‰) and equal to modern snow values from the Antarctic Peninsula (Masson-Delmotte et al., 2008). This result is initially surprising considering the shift in climate regime from temperate in the Paleogene to polar in the present day. However, precipitation changes at the coast are often minimal, as demonstrated by comparison of modern and modelled precipitation isotope gradients used to interpret late Eocene samples from the margins of the Antarctic Peninsula (Feakins et al., 2014). Thus, we infer from δD values that biomarkers in JPC-54 and -55 were most likely sourced locally from plants in the proximal coastal lowland regions of the Sabrina Coast, as more D-depleted values would be expected for biomarkers sourced from farther inland or higher elevations (Masson-Delmotte et al., 2008).

Further support for a local plant source comes from the presence of plant wax *n*-alkanoic acids, which have high abundances of C_{16} and C_{18} that indicate fresh biomass inputs (likely aquatic production) and high CPI long chain plant derived *n*-alkanoic acids, which indicate fresh inputs of those biomarkers without thermal alteration (Fig. 13). Plant wax *n*-alkanoic acids are likely sourced from wind or fluvial transport from the adjacent continent. Modern studies of catchment sourcing are not possible in Antarctica today, given ice cover. However, studies elsewhere show that, while rivers are catchment integrators, plant waxes are typically derived from lowland sources, due to the generally greater areal extent of lowlands and their proximity to the continental shelf, where these compounds are generally deposited; proximal sourcing is especially prominent for the *n*-alkanoic acids (Galy et al., 2011; Hemingway, et al., 2016; Feakins et al., 2018). Studies of modern temperate forest tree leaves in Chile noted that the *n*-alkanoic acids were more abundant than *n*-alkanes in *Nothofagus*

dombeyi (Cerda-Peña et al., 2020), supporting plant inputs of these long chain *n*-alkanoic acids from ancient *Nothofagus* spp.

Plant wax $\delta^{13}C$ provides further insight into the hydroclimate of the Sabrina Coast. Water supply is the dominant factor affecting carbon isotope fractionation in plants (Diefendorf et al., 2010). For the plant waxes analyzed in Sabrina shelf sediments, $\delta^{13}C_{30}$ values from JPC-54 (–31 to –29‰) are compared to the global distribution of modern $\delta^{13}C$ from leaf waxes in a range of climatic conditions (Diefendorf and Freimuth, 2017). The more positive $\delta^{13}C$ values obtained here are best explained as being derived from open habitats (not closed canopy) and/or tundra conditions, with reduced discrimination against ^{13}C likely due to low moisture availability (Diefendorf et al., 2010). The $\delta^{13}C$ values are inconsistent with a closed canopy woodland, where respired CO_2 leads to more depleted ^{13}C values. These $\delta^{13}C$ values and climatic interpretation are consistent with the few Paleogene records from Antarctica, including the $\delta^{13}C_{30}$ from ODP Site 1166 in Prydz Bay (Units III and IV: –28 to –25‰; Tibbett et al., 2021) and pollen $\delta^{13}C$ from the Antarctic Peninsula (Griener et al., 2013). While the long chain *n*-alkanoic acids in proximal marine sediments are dominantly plant derived, with similar distributions noted in extant *Nothofagus* elsewhere (Cerda-Peña et al., 2020), shorter chain lengths may have microbial sources (Chen et al., 2019), as corroborated by their higher $\delta^{13}C$ values. However, we cannot rule out some contribution from microbial sources to the C_{30} *n*-alkanoic acids (Chen et al., 2019), but they are most likely plant derived based on the abundant pollen described here.

The presence of abundant, 'fresh' or penecontemporaneous *n*-alkanoic acids and lesser amounts of low CPI *n*-alkanes and partially matured hopanes detected in Sabrina Coast shelf sediments indicate both penecontemporaneous inputs of plant materials as well as an admixed component of reworked materials (Fig. 13). We can discount the possibility of thermal alteration *in situ,* as *n*-alkanoic acids would not be preserved. We therefore suggest that JPC-54 and -55 contain alkanes and hopanes derived from older, mature sediments that were likely eroded from the Sabrina and Aurora Basins and deposited on the Sabrina Coast shelf, in conjunction with long chain *n*-alkanoic acids that reflect penecontemporaneous vegetation inputs, similar to the biomarker findings and interpretations in other marginal settings around Antarctica (Duncan et al., 2019; Tibbett et al., 2021). It is the combination of evidence for both fresh and reworked components in both the biomarkers and pollen studies, also described in other Antarctic marginal sediments (Tibbett et al., 2021), that are particularly compelling. Here, the biomarker mixtures echo that of the palynology with evidence for both penecontemporaneous and reworked pollen (Smith et al., 2019) as well as lignite in JPC-55

Unit II sediments (Gulick, Shevenell et al., 2017). We do not find any evidence that the sediments in these short cores are homogenous, as might occur through mixing, as many of the biomarker proxies show considerable variability in abundance and in some of the measured indices, although isotopes are invariant (Fig. 13).

To assess reworking in the short Sabrina Coast sedimentary sequences, we studied the palynomorphs in the late Quaternary-age Unit I of JPC-54 and -55 as well as the late Miocene to Pliocene sediments recovered in JPC-30 and -31 (Gulick, Shevenell et al., 2017). In Unit I and in JPC-30 and -31, palynomorphs are in low abundance and correspondence analysis indicate that these statistical groups (G1, 54-1, and 55-1) are similar and may be at least partially derived from the same sedimentary source (Fig. 11).

4.2. Sabrina Coast paleoenvironments

The Sabrina Flora is a unique assemblage, with high abundances of *Gambierina* spp., *Battenipollis* spp., and Proteaceae (Figs. 5, 7). Low abundances of *Nothofagidites* spp. (<10%) make the Sabrina Flora distinct from other Antarctic margin records, where *Nothofagidites* spp. dominate assemblages (e.g., Askin, 1988; Francis et al., 2009; Truswell and Macphail, 2009; Anderson et al., 2011; Warny and Askin, 2011; Contreras et al., 2013). The high abundances of palynomorphs with unknown botanical affinities make environmental reconstruction based on the Sabrina Flora alone difficult. A multi-proxy approach can provide insights into the Late Cretaceous to Cenozoic evolution of paleoenvironmental conditions on the Sabrina Coast. These insights will likely evolve as longer records are recovered by drilling, dating is refined, and reworking is assessed. However, short cores collected from the Sabrina Coast provide a unique first glimpse at the region's pre-glacial to glacial paleoenvironment (Gulick, Shevenell et al., 2019; Smith et al., 2019; Macphail et al., 2020).

Sediment core JPC-55 was collected from a seismically stratified facies with subparallel reflectors, 15-20 m below the youngest of a series of progradational wedge-shaped clinoforms interpreted as deltas of fluvial and/or glaciofluvial origin, suggesting regression-transgression sequences that reflect changes in relative sea level and/or sediment flux to the shelf (Gulick, Shevenell et al., 2017; Montelli et al., 2020). The seismic signature, coupled with comparisons to previously drilled Antarctic margin sequences (e.g., McKay et al., 2019) indicate that JPC-55 was recovered from an ice-distal hemipelagic sedimentary sequence seaward of a low lying fluvial coastal plain (Young et al., 2011; Aitken et al., 2016; Gulick, Shevenell et al., 2017; Montelli et al., 2020). Preliminary age assessments indicate that JPC-55 contains sediments of Paleocene age (Gulick, Shevenell et al., 2017; Smith et al., 2019);

this estimate will be further refined when longer sedimentary sequences are recovered from the Sabrina Coast margin (Macphail, 2021; McKay et al., 2021). The Sabrina Flora assemblage in JPC-55 Unit II (groups 55-2 and 55-3; Fig. 6) is dominated by *G. askinae* and *B. sabrinae* with unusually rugulate sculptured exines, relatively high abundances of *P. parvus* (4.7%), low abundances of *Nothofagidites* spp., and relatively low cryptogam spore abundances (3.2-9.5%). Taken together, the assemblage is consistent with limited plant moisture availability and a moderately dry environment (Griener et al., 2013). A complicating factor is that the dominant species in the Sabrina Flora (e.g., *Gambierina*, *Battenipollis*, *Forcipites)* have no known botanical affinities or relationships with modern Austral flora. Dettmann and Jarzen (1988) suggested that *Gambierina*, *Battenipollis*, and *Forcipites* may have inhabited a forest environment adjacent to an estuary. Correspondence analysis shows *B. sectilis* and *F. stipulatus* likely inhabited similar environments to *P. parvus,* which typically indicates open, shrubby environments (Bowman et al., 2014). In total, the palynomorph, seismic data (Gulick, Shevenell, et al. 2017; Montelli et al., 2020), subglacial topography and geomorphology (Young et al., 2011; Aitken et al., 2016), and plant wax $\delta^{13}C$ data suggest that a moderately dry open coastal vegetation existed along the Sabrina Coast in the Late Cretaceous (Macphail, 2021) to early Paleogene (Gulick, Shevenell et al., 2017; Smith et al., 2019), and that terrestrial sediment was likely transported to the shelf by fluvial processes. Core JPC-54, dated to the early to middle Eocene, was recovered 13 m above the youngest clinoform, and 25-30 m above JPC-55, from a seismic facies with moderate laterally variable reflectors indicative of a more ice-proximal setting, but one where ice had not yet advanced across the continental shelf. Lonestones recovered in JPC-54 are interpreted as ice rafted debris, indicative of marine terminating ice along the Sabrina coast (Gulick, Shevenell et al., 2017; Smith et al, 2019; Montelli et al., 2020). The palynomorph assemblage in JPC-54 differs significantly from that of JPC-55, as it is dominated by *G. rudata* (Fig. 7). This species exhibits a smooth exine structure as compared to the rugulate species dominant in the JPC-55 assemblage. The JPC-54 assemblage has higher abundances of *N. lachlaniae* (4.6%) compared to JPC-55 (1.7%). Correspondence analysis shows *N. lachlaniae* plotting together with *L. ovatus*, *Liliacidites* spp., Proteaceae, and *Arecipites* spp. (Fig. 12). This correlation could be indicative of a complex open forest environment containing relatively high abundances of both overstory (i.e., *Nothofagus* and *Arecipites* [palms]) and understory (i.e., ferns, including *L. ovatus*) vegetation. *Nothofagidites* spp. abundances are slightly higher than in JPC-55, although still relatively low when compared with Eocene sequences in the Antarctic Peninsula, Transantarctic Mountains, Prydz Bay, and Wilkes Land (e.g., Askin,

1988; Francis et al., 2009; Truswell and Macphail, 2009; Anderson et al., 2011; Warny and Askin, 2011; Contreras et al., 2013). Cryptogam spore abundances remain relatively low (4.6-15.7%), but higher than in JPC-55. Taken together, the palynological data from JPC-54 suggest a more humid Sabrina Coast environment with an open canopy forest in the early to middle Eocene. However, the average plant wax alkanoic acid $\delta^{13}C$ value (30.2 ± 0.5‰) and low abundances of spores and *Nothofagidites* spp. suggest that regional conditions were still relatively dry. The co-existence of marine-terminating glaciers (Gulick, Shevenell et al., 2017) and an ecosystem with highly diverse vegetation could be indicative of an environment similar to modern-day Patagonia, southern New Zealand, or southeast Alaska.

5. Conclusions

The Sabrina Flora is composed of a unique assemblage never previously recovered from Antarctica. Detailed species distribution results and new statistical analyses were performed on the assemblage and discussed to extrapolate potential paleoenvironmental affinities of *Battenipollis sabrinae* and *Gambierina askiniae*, the two recently described species that dominate the assemblage (Smith et al., 2019). We add analysis of biomarkers to find evidence for penecontemporaneous and reworked components of the biomarkers as a mixture in these sediments, from which we can interpret the *in situ* component (*n*-alkanoic acids) for signals of paleoenvironment. The palynomorph assemblage and plant wax *n*-alkanoic acid $\delta^{13}C$ values suggest that the Sabrina Flora represents an open canopy woodland or shrubby environment. Pollen assemblage differences between the older JPC-55 and younger JPC-54 suggest a shift in vegetation and climate from somewhat drier shrubby, open vegetation (JPC-55) to a more open canopy forest (JPC-54). Global climate trends may play a role in this change in vegetation as well as potential influence from the opening of the Tasman gateway. However, improved age controls will be necessary for further interpretations. This study highlights the need for longer sedimentary sequences from East Antarctica, both from the continental shelf and from proximal subglacial basins. Such records will enable researchers to assess the impact of reworking on proximal sequences, increase chronological confidence, and improve understanding of Late Cretaceous to Recent paleoenvironments in the Aurora and Wilkes Subglacial Basins.

Acknowledgements

Core acquisition during NBP14-02 was supported by the National Science Foundation Antarctic Integrated Systems Science Project (grants NSF PLR1143836, PLR-1143837, PLR-

1143843, PLR-1430550, and PLR-1048343). We thank the NBP14-02 crew and scientific party for their roles in collecting the samples. Processing of all palynologic samples was funded by US NSF CAREER grant ANT-1048343 to S. Warny. Plant wax work was funded by NSF-OPP-1908548 to S. Feakins.

References

Aitken, A., Roberts, J., Ommen, T., Young, D.A., Golledge, N.R., Greenbaum, J.S., Blankenship, D.D., Siegert, M.J., 2016. Repeated large-scale retreat and advance of Totten Glacier indicated by inland bed erosion. Nature 533, 385–389.

Anderson, J.B., Warny, S., Askin, R.A., Wellner, J.S., Bohaty, S.M., Kirshner, A.E., Livsey, D.N., Simms, A.R., Smith, T.R., Ehrmann, W. Lawver, L.A., 2011. Progressive Cenozoic cooling and the demise of Antarctica's last refugium. Proceedings of the National Academy of Sciences 108, 11356–11360.

Askin, R.A., 1988. Campanian to Paleocene palynological succession of Seymour and adjacent islands, northeastern Antarctic Peninsula. In: Feldman, R.M., Woodburne, M.O. (eds), Geology and Paleontology of Seymour Island, Antarctic Peninsula. Geological Society of America Memoir 169, pp. 131–153.

Askin, R.A., 2000. Spores and pollen from the McMurdo Sound erratics, Antarctica. AGU Antarctic Research Series 76, 161–181.

Bakkelund, A., Porter, T.J., Froese, D.G., Feakins, S.J., 2018. Net fractionation of hydrogen isotopes in n-alkanoic acids from soils in the northern boreal forest. Organic Geochemistry 125, 1–13.

Baudoin, P., 2018. Reconstruction of Antarctic Cenozoic Paleoenvironments Through Palynological Analysis of Subglacial Lake and Ice Stream Sediments. LSU Master's thesis (Unpubl.) (https://digitalcommons.lsu.edu/gradschool_theses/4721/).

Bijl, P.K. Bendle, J.A.P., Bohaty, S.M., Pross, J., Schouten, S., Tauxe, L., Stickley, C.E., McKay, R.M., Röhl, U., Olney, M., Sluijs, A., Escutia, C., Brinkhuis, H., Expedition 318 Scientists, 2013. Eocene cooling linked to early flow across the Tasmanian Gateway. Proceedings of the National Academy of Science 110, 9645–9650.

Bowman, V.C., Francis, J.E., Askin, R.A., Riding, J.B., Swindles, G.T., 2014. Latest Cretaceous-earliest Paleogene vegetation and climate change at the high southern latitudes: palynological evidence from Seymour Island, Antarctic Peninsula. Palaeogeography, Palaeoclimatology, Palaeoecology 408, 26–47.

Cande, S.C., Mutter, J.C., 1982. A Revised Identification of the Oldest Sea-Floor Spreading Anomalies between Australia and Antarctica. Earth and Planetary Science Letters 58, 151–160.

Cerda-Peña, C., Contreras, S., Rau, J.R., 2020. Molecular n-alkyl leaf waxes of three dominant plants from the temperate forest in South America. Organic Geochemistry 149, 104105.

Chen, X., Liu, X., Wei, Y., Huang, Y., 2019. Production of long-chain n-alkyl lipids by heterotrophic microbes: new evidence from Antarctic lakes. Organic Geochemistry 138, 103909.

Clarke, K.R., 1993. Non-parametric multivariate analyses of changes in community structure. Australian Journal of Ecology 18, 117–143.

Coenen, J.J., Scherer, R., Baudoin, P., Warny, S., Castañeda, I.S., Askin, R., 2019. Paleogene marine and terrestrial development of the West Antarctic Rift System. Geophysical Research Letters 47, e2019GL085281.

Contreras, L., Pross, J., Bijl, P.K., Koutsodendris, A., Raine, J.I., van de Schootbrugge, B., Brinkhuis, H., 2013. Early to middle Eocene vegetation dynamics at the Wilkes Land Margin (Antarctica). Review of Palaeobotany and Palynology 197, 119–142.

Contreras, L., Pross, J., Bijl, P.K., O'Hara, R.B., Raine, J.I., Sluijs, A., Brinkhuis, H., 2014. Southern high-latitude terrestrial climate change during the Palaeocene-Eocene derived from a marine pollen record (ODP 1172, East Tasman Plateau). Climate of the Past 10, 1401–1420.

Cookson, I.C., 1950. Fossil pollen grains of Proteaceous type from Tertiary deposits in Australia. Australian Journal of Science, series B 3, 166–177.

Cookson, I.C., Pike, K.M., 1954. Some dicotyledonous pollen types from Cainozoic deposits in the Australian region. Australian Journal of Botany 2, 197–219.

Couper, R.A., 1960. New Zealand Mesozoic and Cainozoic plant microfossils. New Zealand Geological Survey Palaeontological Bulletin 32, 87 p.

Coxall, H.K., Wilson, P.A., Pälike, H., Lear, C.H., Backman, J., 2005. Rapid stepwise onset of Antarctic glaciation and deeper calcite compensation in the Pacific Ocean. Nature 433, 53–57.

DeConto, R.M., Pollard, D., 2016. Contribution of Antarctica to past and future sea-level rise. Nature 531, 591–597.

Dettmann, M. E., Jarzen, D. M., 1988. Angiosperm pollen from uppermost Cretaceous strata of southeastern Australia and the Antarctic Peninsula. Memoirs of the Association of Australasian Palaentologists 5, 217–237.

Diefendorf, A.F., Mueller, K.E., Wing, S.L., Koch, P.L., Freeman, K.H., 2010. Global patterns in leaf ^{13}C discrimination and implications for studies of past and future climate. Proceedings of the National Academy of Science 107, 5738–5743.

Diefendorf, A.F., Freimuth, E.J., 2017. Extracting the most from terrestrial plant-derived *n*-alkyl lipids and their carbon isotopes from the sedimentary record: A review. Organic Geochemistry 103, 1–21.

Duncan, B., McKay, R., Bendle, J., Naish, T., Inglis, G.N., Moossen, H., Levy, R., Ventura, G.T., Lewis, A., Chamberlain, B., Walker, C., 2019. Lipid biomarker distributions in Oligocene and Miocene sediments from the Ross Sea region, Antarctica: Implications for use of biomarker proxies in glacially-influenced settings. Palaeogeography, Palaeoclimatology, Palaeoecology 516, 71–89.

Escutia, C., Brinkhuis, H., Klaus, A., the IODP Expedition 318 Scientists, 2011. IODP expedition 318: From greenhouse to icehouse at the Wilkes Land Antarctic margin. Scientific Drilling 12, 15–23.

Feakins, S.J., Warny, S., Lee, J., 2012. Hydrologic cycling over Antarctica during the middle Miocene warming. Nature Geoscience 5, 557–560.

Feakins, S.J., Warny, S., DeConto, R.M., 2014. Snapshot of cooling and drying before onset of Antarctic Glaciation. Earth and Planetary Science Letters 404, 154–166.

Feakins, S.J., Wu, M.S., Ponton, C., Galy, V., West, A.J., 2018. Dual isotope evidence for sedimentary integration of plant wax biomarkers across an Andes-Amazon elevation transect. Geochimica et Cosmochimica Acta 242, 64–81.

Francis, J.E., 2000. Fossil wood from Eocene high latitude forests McMurdo Sound, Antarctica. AGU Antarctic Research Series 76, 253–260.

Francis, J.E., Marenssi, S., Levy, R., Hambrey, M., Thorn, V.C., Mohr, B., Brinkhuis, H., Warnaar, J., Zachos, J., Bohaty, S., DeConto, R., 2009. From greenhouse to icehouse–the Eocene/Oligocene in Antarctica. Developments in Earth and Environmental Science 8, 309–368.

Fretwell, P., Pritchard, H.D., Vaughan, D.G., Bamber, J.L., Barrand, N.E., Bell, R., Bianchi, C., Bingham, R.G., Blankenship, D.D., Casassa, G., Catania, G., Callens, D., Conway, H., Cook, A.J., Corr, H.F.J., Damaske, D., Damm, V., Ferraccioli, F., Forsberg, R., Fujita, S., Gogineni, P., Griggs, J.A., Hindmarsh, R.C.A., Holmlund, P., Holt, J.W.,

Jacobel, R.W., Jenkins, A., Jokat, W., Jordan, T., King, E.C., Kohler, J., Krabill, W., Riger-Kusk, M., Langley, K.A., Leitchenkov, G., Leuschen, C., Luyendyk, B.P., Matsuoka, Mouginot, K.J., Nitsche, F.O., Nogi, Y., Nost, O.A., Popov, S.V., Rignot, E., Rippin, D.M., Rivera, A., Roberts, J., Ross, N., Siegert, M.J., Smith, A.M., Steinhage, D., Studinger, M., Sun, B., Tinto, B.K., Welch, B.C., Wilson, D., Young, D.A., Xiangbin, C., Zirizzotti, A., 2013. Bedmap2: improved ice bed, surface and thickness datasets for Antarctica. The Cryosphere 7, 375–393.

Galy, V., Eglinton, T., France-Lanord, C., Sylva, S., 2011. The provenance of vegetation and environmental signatures encoded in vascular plant biomarkers carried by the Ganges-Brahmaputra rivers. Earth and Planetary Science Letters 304, 1–12.

Greenbaum, J.S., Blankenship, D., Young, A., Richter, T.G., Roberts, J.L., Aitken, A.R.A., Legresy, B., Schroeder, D.M., Warner, R.C., van Ommen, T.D., Siegert, M.J., 2015. Ocean access to a cavity beneath Totten Glacier in East Antarctica. Nature 8, 294–298.

Greenwood, D.R., Moss, P.T., Rowett, A.I., Vadala, A.J., Keefe, R.L., 2003. Plant communities and climate change in southeastern Australia during the early Paleogene. Special Papers on Geological Society of America 369, 365–380.

Griener, K.W., Nelson, D.M., Warny, S., 2013. Declining moisture availability on the Antarctic Peninsula during the late Eocene. Palaeogeography, Palaeoclimatology, Palaeoecology 383, 72–78.

Gulick, S.P.S., Shevenell, A.E., Montelli, A., Fernandez, R., Smith, C., Warny, S., Bohaty, A.M., Sjunneskog, C., Leventer, A., Frederick, B., Blankenship, D.D., 2017. Initiation and long-term instability of the East Antarctic Ice Sheet. Nature 552, 225–229.

Hammer, Ø., Harper, D., Ryan, P., 2001. PAST: paleontological statistics software package for education and data analysis. Palaeontologia Electronica 4, 9 p.

Hemingway, J.D., Schefuß, E., Dinga, B.J., Pryer, H., Galy, V.V., 2016. Multiple plant-wax compounds record differential sources and ecosystem structure in large river catchments. Geochimica et Cosmochimica Acta 184, 20–40.

Hou, B., Alley, N.F., Frakes, L.A., Stoian, L, Cowley, W.M., 2006. Eocene stratigraphic succession in the Eucla Basin of South Australia and correlation to major regional sea-level events. Sedimentary Geology 183, 297–583.

Inglis, G.N., Naafs, B.D.A., Zheng, Y., McClymont, E.L., Evershed, R.P., Pancost, R.D., 2018. Distributions of geohopanoids in peat: Implications for the use of hopanoid-based proxies in natural archives. Geochimica et Cosmochimica Acta 224, 249–261.

Inglis, G.N., Carmichael, M.J., Farnsworth, A., Lunt, D.J., Pancost, R.D., 2020. A long-term, high-latitude record of Eocene hydrological change in the Greenland region. Palaeogeography, Palaeoclimatology, Palaeoecology 537, 109378.

Jarzen, D.M., Dettmannn, M.E., 1992. Structure and form of austral Cretaceous Normapolles-like pollen. Geobios 25, 569–583.

Kennett, J.P., 1977. Cenozoic evolution of Antarctic glaciation, the Circum Antarctic Ocean, and their impact on global paleoceanography. Journal of Geophysical Research 82, 3843–3860.

Lear, C.H., Elderfield, H., Wilson, P.A., 2000. Cenozoic deep-sea temperatures and global ice volumes from Mg/Ca in benthic foraminiferal calcite. Science 287, 269–272.

Legendre, P., Legendre, L., 2012. Numerical ecology, 3rd Edition. Developments in Environmental Modelling 24, 1006 p.

Levy, R.H., Harwood, D.M., 2000. Tertiary marine palynomorphs from the McMurdo Sound erratics, Antarctica. AGU Antarctic Research Series 76, 183–242.

Lewis, A.R., Marchant, D.R., Ashworth, A.C., Hedenäs, L., Hemming, S.R., Johnson, J.V., Leng, M.J., Machlus, M.L., Newton, A.E., Raine, I., Willenbring, J.K., Williams, M., Wolfe, A.P., 2008. Mid-Miocene cooling and the extinction of tundra in continental Antarctica. Proceedings of the National Academy of Science 105, 10676–10680.

Macphail, M.K., 2021. The Sabrina Floras of East Antarctica: Late Cretaceous, Paleogene or reworked? Palynology 45, 745–752.

Macphail, M.K., Truswell, E.M., 2004. Palynology of Neogene slope and rise deposits from ODP Sites 1165 and 1167, East Antarctica. In: Cooper, A.K.; O'Brien, P.E., Richter, C. (eds), Proceedings of the Ocean Drilling Program, scientific results, volume 188, pp. 1–20.

Masson-Delmotte, V., Hou, S., Ekaykin, A., Jouzel, J., Aristarain, A., Bernardo, R.T., Bromwich, D., Cattani, O., Delmotte, M., Falourd, S., Frezzotti, M., Gallée, H., Genoni, L., Isaksson, E., Landais, A., Helsen, M.M., Hoffmann, G., Lopez, J., Morgan, V., Motoyama, N., Noone, D., Oerter, H., Petit, J.R., Royer, A., Uemura, R., Schmidt, G.A., Schlosser, E., Simöes, J.C., Steig, E.J., Stenni, B., Stievenard, M., van den Broeke, M.R., van de Wal, R.S.W., van de Berg, W.J., Vimeux, F., White, J.W.C., 2008. A review of Antarctic surface snow isotopic composition: Observations, atmospheric circulation, and isotopic modeling. Journal of Climate 21, 3359–3387.

McFarlin, J.M., Axford, Y., Masterson, A.L., Osburn, M.R., 2019. Calibration of modern sedimentary δ2H plant wax-water relationships in Greenland lakes. Quaternary Science Reviews 225, 105978.

Montelli, A., Gulick, S., Fernandez-Vasquez, R., Frederick, B., Shevenell, A., Leventer, A., Blankenship, D., 2019. Seismic stratigraphy of the Sabrina Coast shelf, East Antarctica: history of early dynamic glaciations. GSA Bulletin 132, 545–561.

Morlighem, M., Rignot, E., Binder, T., Blankenship, D., Drews, R., Eagles, G., 2020. Deep glacial troughs and stabilizing ridges unveiled beneath the margins of the Antarctic ice sheet. Nature Geoscience 13, 132–137.

Partridge, A.D., 2006. Late Cretaceous–Cenozoic palynology zonations, Gippsland Basin. In: Monteil, E. (coord.), Australian Mesozoic and Cenozoic Palynology Zonations.

Pross, J., Contreras, L., Bijl, P.K., Greenwood, D.R., Bohaty, S.M., Schouten, S., Bendle, J.A., Rohl, U., Trauze, L., 2012. Persistent near-tropical warmth on the Antarctic continent during the Early Eocene epoch. Nature 488, 73–77.

Raine, J.I., 1984. Outline of a palynological zonation of Cretaceous to Paleogene terrestrial sediments in west coast region, South Island, New Zealand. Republic of New Zealand Geological Survey 109, 1–82.

Raine, J.I., Mildenhall, D.C., Kennedy, E.M., 2011. New Zealand fossil spores and pollen: an illustrated catalogue. 4th edition. GNS Science miscellaneous series no. 4. (http://data.gns.cri.nz/sporespollen/index.htm).

Rau, D., 2017. In search of Antarctica's last vegetation refugium within the McMurdo Dry Valleys. LSU Master's Thesis (Unpubl.), (https://digitalcommons.lsu.edu/gradschool_theses/4468/).

Sessions, A.L., Zhang, L., Welander, P.V., Doughty, D., Summons, R.E., Newman, D.K., 2013. Identification and quantification of polyfunctionalized hopanoids by high temperature gas chromatography-mass spectrometry. Organic Geochemistry 56, 120–130.

Smith, C., 2016. An Early Paleogene Palynological Assemblage from the Sabrina Coast, East Antarctica: New Species and Implications for Depositional History. University of South Florida Master's thesis (Unpubl.).

Smith, C., Warny, S., Shevenell, A.E., Gulick, S.P.S., Leventer, A., 2019. New species from the Sabrina Flora: an early Paleogene pollen and spore assemblage from the Sabrina Coast, East Antarctica. Palynology 43, 650–659.

Stover, L.E., Partridge, A.D., 1973. Tertiary and Late Cretaceous spores and pollen from the Gippsland Basin, southeastern Australia. Proceedings of the Royal Society of Victoria 85, 237–286.

Tibbett, E.J., Scher, H.D., Warny, S., Tierney, J.E., Passchier, S., Feakins, S.J., 2021. Late Eocene Record of Hydrology and Temperature From Prydz Bay, East Antarctica. Paleoceanography and Paleoclimatology 36, e2020PA004204.

Truswell, E.M., 1983. Recycled Cretaceous and Tertiary pollen and spores in Antarctic marine sediments: a catalogue. Palaeontographica Abteilung B 186, 121–174.

Truswell, E.M., 1997. Palynomorph assemblages from marine Eocene sediments on the west Tasmanian continental margin and the South Tasman Rise. Australian Journal of Earth Sciences 44, 633–654.

Truswell, E.M., Macphail, M.K., 2009. Polar forests on the edge of extinction: what does the fossil spore and pollen evidence from East Antarctica say? Australian Systematic Botany 22, 57–106.

Uemura, H., Ishiwatari, R., 1995. Identification of unusual 17β(H)-moret-22(29)-ene in lake sediments. Organic Geochemistry 23, 675–680.

Warny S., Askin, R., 2011. Vegetation and organic-walled phytoplankton at the end of the Antarctic greenhouse world: latest cooling events. AGU Special Publication 63, 193–210.

Warny, S., Kymes, C.M., Askin, R., Krajewski, K.P., Tatur, A., 2019. Terrestrial and marine floral response to latest Eocene and Oligocene events on the Antarctic Peninsula. Palynology 43, 4–21.

Wilkie, K.M.K., Chapligin, B., Meyer, H., Burns, S., Petsch, S., Brigham-Grette, J., 2013. Modern isotope hydrology and controls on δD of plant leaf waxes at Lake El'gygytgyn, NE Russia. Climate of the Past 9, 335–352.

Wright, A.P., Young, D.A., Roberts, J.L., Schroeder, D.M., Bamber, J.L., Dowdeswell, J.A., Young, N.W., Le Brocq, A.M., Warner, R.C., Payne, A.J., Blankenship, D.D., van Ommen, T.D., Siegert, M.J., 2012. Evidence of a hydrological connection between the ice divide and ice sheet margin in the Aurora Subglacial Basin, East Antarctica. Journal of Geophysical Research 117, F01033.

Young, D.A., Wright, A.P., Roberts, J.L., Warner, R.C., Young, N.W., Greenbaum, J.S., Schroeder, D.M., Holt, J.W., Sugden, D.E., Blankenship, D.D., van Omen, T.D., Siegert, M.J., 2011. A dynamic early East Antarctic Ice Sheet suggested by ice-covered fjord landscapes. Nature 474, 72–75.

Zachos, J., Pagani, M., Sloan, L., Thomas, E., Billups, K., 2001. Trends, rhythms, and aberrations in global climate 65 Ma to present. Science 292, 686–693.

Zachos, J., Dickens, G.R., Zeebe, R.E., 2008. An early Cenozoic perspective on greenhouse warming and carbon-cycle dynamics. Nature 451, 279–283.

Table and Figure captions

Table 1. Four-group SIMPER analysis with Bray-Curtis similarity matrix conducted for groups G1, G2, G3, and G4. “Taxa A” taxa account for 50.5% of compositional variability between the four groups. “Taxa B” and “Taxa C” taxa together explain 30% of compositional variability. These three groups together account for 80.5% of compositional differences between the four groups.

Figure 1. Paleogeographic reconstruction for the Australian-Antarctic margins at 50 Ma. Aurora Subglacial Basin and Eucla Basin are outlined in blue. Study location indicated by a star.

Figure 2. Bathymetry of Sabrina Coast continental shelf, mapped during NBP14-02 using a Kongsberg EM 120 multibeam system. Locations of JPC-30, 31, 54 and 55 are denoted by blue circles. Black line represents seismic line 17. Modified from Smith et al. (2018).

Figure 3. Core photos, core x-rays, lithologies and sample distributions for JPC-54, 55, 30 and 31.

Figure 4. UPGMA cluster analysis of a Bray-Curtis similarity matrix with no stratigraphic constraint. Y-axis shows similarity level between samples. Samples are indicated by JPC#-Unit#-Depth (cm) with JPC-54 shown in blue, JPC-55 in red, JPC-30 in green and JPC-31 in brown.

Figure 5. Palynomorph absolute and relative abundances, Shannon Diversity Index and assemblage data from JPC-55 (MS-III, older core). Relative abundances of *G. rudata*, *G. askinae*, *B. sectilis*, *B. sabrinae*, *Forcipites* spp., *Proteacidites* spp., *Nothofagidites* spp., *L. ovatus* and Gymnosperms are shown. Unit I (orange shading) consists of late Pleistocene to Holocene glaciomarine sandy silt with low palynomorph abundances. Unit II (yellow shading) consists of organic-rich silty sand containing the diverse Sabrina Flora assemblage. Note that Unit I relative abundance curves are not a reflection of vegetation change, but are proportions of a very sparse, reworked assemblage.

Figure 6. UPGMA cluster analysis of a Bray-Curtis similarity matrix with stratigraphic constraint for all samples in JPC-55. Y-axis shows similarity level between samples. Sample depth is shown horizontally. Group 55-1 contains all samples from JPC-55, Unit I. Groups 55-2 and 55-3 contain samples from JPC-55, Unit II. Groups 55-1, 55-2 and 55-3 are all statistically different (ANOSIM test), indicating a clear distinction in palynomorph assemblage between Unit I and II, as well as a change in assemblage within Unit II.

Figure 7. Palynomorph absolute and relative abundances, Shannon Diversity Index and assemblage data from JPC-54 (MS-III, younger core). Relative abundances of *G. rudata*, *G. askinae*, *B. sectilis*, *B. sabrinae*, *Forcipites* spp., *Proteacidites* spp., *Nothofagidites* spp., *L. ovatus* and gymnosperms are shown. Unit I (orange shading) consists of late Pleistocene to Holocene glaciomarine sandy silt with low palynomorph abundances. Unit II (yellow shading) consists of organic-rich silty sand containing the diverse Sabrina Flora assemblage. Note that Unit I relative abundance curves are not a reflection of vegetation change, but are proportions of a very sparse, reworked assemblage.

Figure 8. UPGMA cluster analysis of a Bray-Curtis similarity matrix with stratigraphic constraint for all samples in JPC-54. Y-axis shows similarity level between samples. Sample depth is shown horizontally. Group 54-1 contains only samples from JPC-54, Unit I. Groups 54-2 and 54-3 contain all samples from JPC-54, Unit II. Group 54-1 is statistically different from groups 54-2 and 54-3, but groups 54-2 and 54-3 are not statistically different from each other (ANOSIM test). This indicates a clear distinction between the palynomorph assemblages of Unit I and Unit II.

Figure 9. Palynomorph abundance, Shannon Diversity Index and relative abundance of dominant species for JPC-30.

Figure 10. Palynomorph abundance, Shannon Diversity Index and relative abundance of dominant species for JPC-31.

Figure 11. Correspondence analysis of JPC-30, JPC-31, JPC-54, and JPC-55 assemblages, using only the 18 major taxa driving the between-group variability (Table 1). Factorial Axis 1 (red) and Factorial Axis 2 (green) account for 50.7% and 21.7% of the overall between-sample variability, respectively. The sparse, reworked assemblages of JPC-30, JPC-31, JPC-

54 Unit I and JPC-55 Unit I group together while the *in situ* assemblages of JPC-54 Unit II and JPC-55 Unit II both plot separately.

Figure 12. Factorial space related to the correspondence analysis shown in Fig. 11. Factorial Axis 1 (red) shows 50.7% of the overall between-sample variation; it is related to changes in abundance of *B. sabrinae* and *G. askinae* vs. *B. sectilis* and *G. rudata.* Factorial Axis 2 (green) shows 21.7% of the overall between-sample variation; it is related to changes in abundance of *B. sectilis*, *Forcipites stipulatus* and *Proteacidites parvus* vs. *L. ovatus*, *N. lachlaniae*, *Liliacidites* spp., *Proteacidites* spp., *Arecipites* spp., and trilete cryptogam spores.

Figure 13. Compilation of biomarker data for Core JPC 54 and 55. **A**. Hopane indices computed for the C_{29} only, C_{31} only, and all hopanoids (C_{27} to C_{31}), showing the direction of greater maturity. **B**. Total plant wax concentrations for both *n*-alkanes (orange) and *n*-alkanoic acids (green). **C**. Average chain length (ACL) of *n*-alkane and *n*-alkanoic acids. **D**. Carbon preference index (CPI) for *n*-alkane and *n*-alkanoic acids, where lower values indicate maturity and higher values indicate fresher or penecontemporary inputs. **E, F**. δD values (E) and $\delta^{13}C$ values (F) for the long chain *n*-alkanoic acids, with putative marine and terrestrial plant contributions denoted.

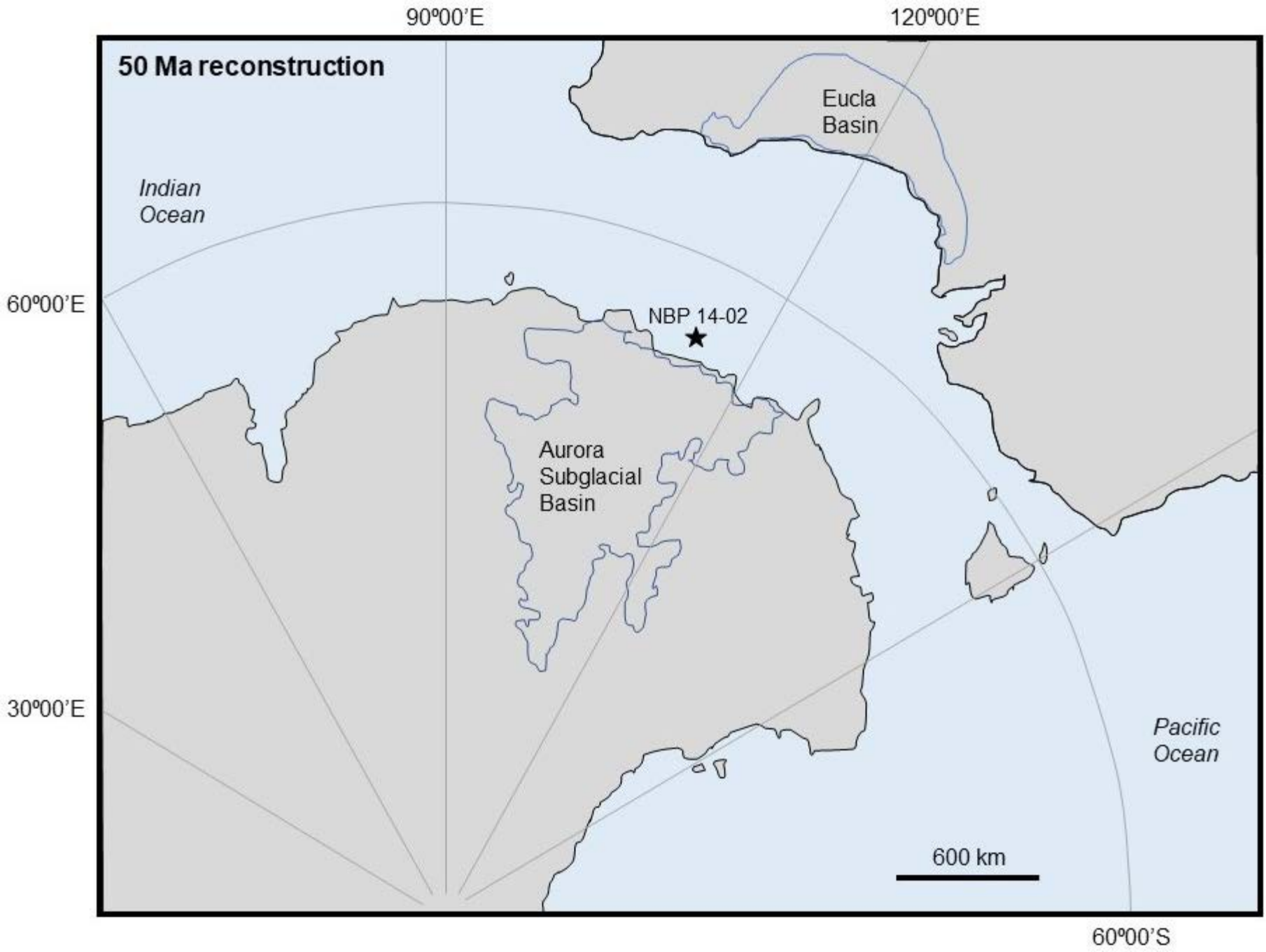
90º00'E
120º00'E
50 Ma reconstruction
Eucla
Basin
Indian
Ocean
60º00'E
NBP 14-02
Aurora
Subglacial
Basin
30º00'E
Pacific
Ocean
600 km
60º00'S

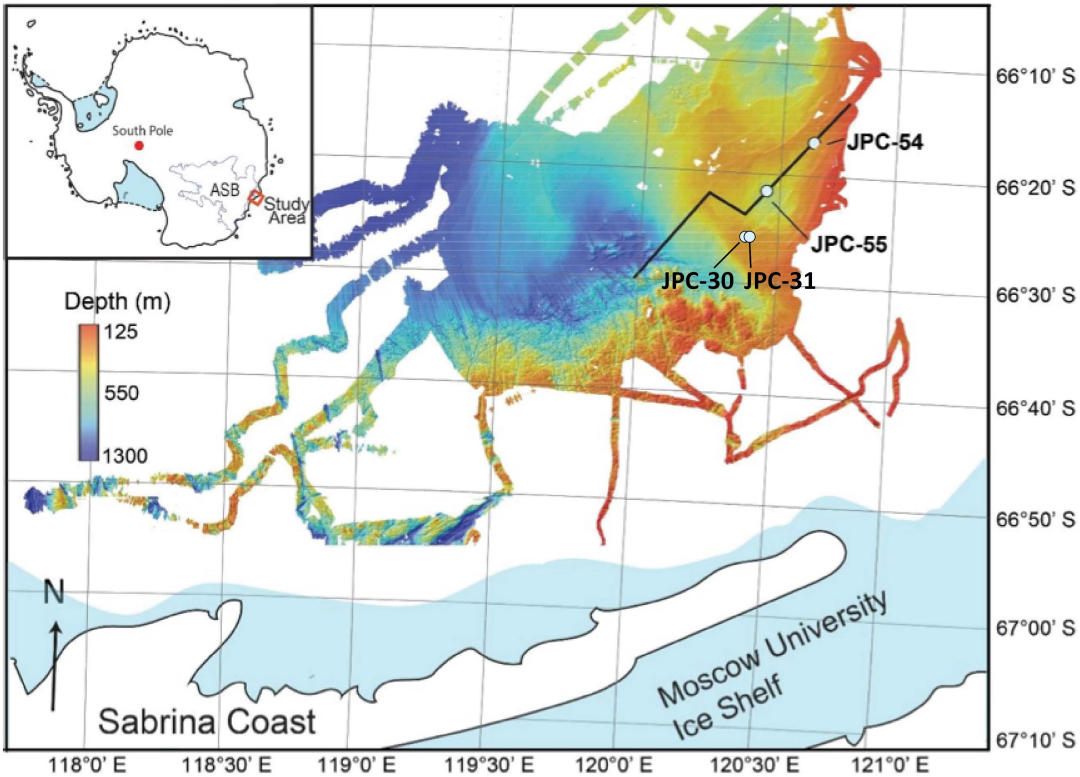
South Pole
ASB
Study Area
Depth (m)
125
550
1300
JPC-54
JPC-55
JPC-30
JPC-31
N
Sabrina Coast
Moscow University Ice Shelf
66°10' S
66°20' S
66°30' S
66°40' S
66°50' S
67°00' S
67°10' S
118°0' E
118°30' E
119°0' E
119°30' E
120°0' E
120°30' E
121°0' E

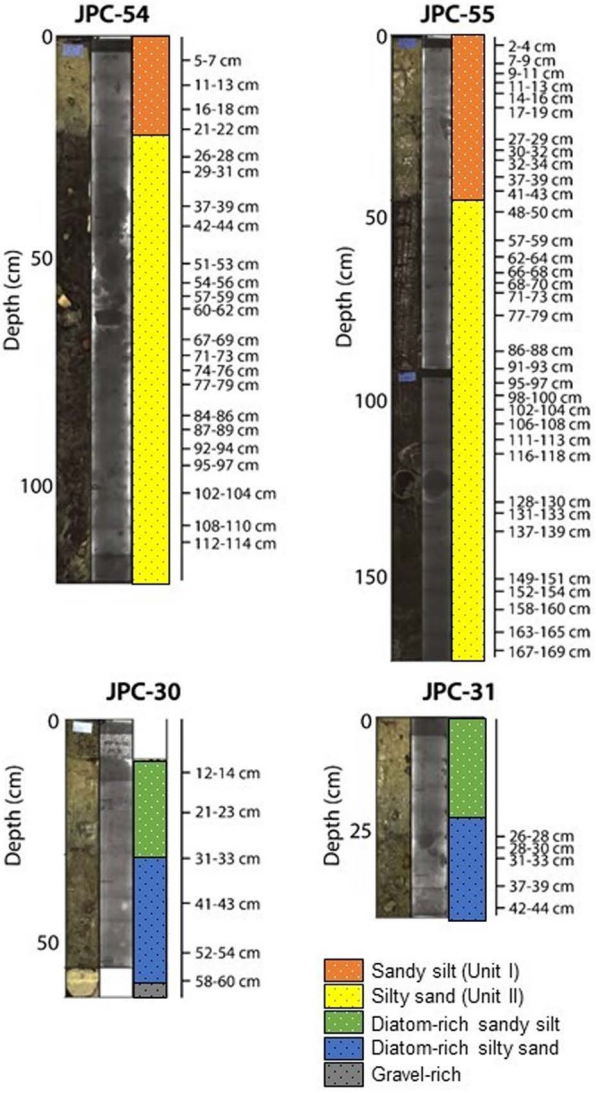
JPC-54
0
50
100
Depth (cm)
5-7 cm
11-13 cm
16-18 cm
21-22 cm
26-28 cm
29-31 cm
37-39 cm
42-44 cm
51-53 cm
54-56 cm
57-59 cm
60-62 cm
67-69 cm
71-73 cm
74-76 cm
77-79 cm
84-86 cm
87-89 cm
92-94 cm
95-97 cm
102-104 cm
108-110 cm
112-114 cm
JPC-55
0
50
100
150
Depth (cm)
2-4 cm
7-9 cm
9-11 cm
11-13 cm
14-16 cm
17-19 cm
27-29 cm
30-32 cm
32-34 cm
37-39 cm
41-43 cm
48-50 cm
57-59 cm
62-64 cm
66-68 cm
68-70 cm
71-73 cm
77-79 cm
86-88 cm
91-93 cm
95-97 cm
98-100 cm
102-104 cm
106-108 cm
111-113 cm
116-118 cm
128-130 cm
131-133 cm
137-139 cm
149-151 cm
152-154 cm
158-160 cm
163-165 cm
167-169 cm
JPC-30
0
50
Depth (cm)
12-14 cm
21-23 cm
31-33 cm
41-43 cm
52-54 cm
58-60 cm
JPC-31
0
25
Depth (cm)
26-28 cm
28-30 cm
31-33 cm
37-39 cm
42-44 cm
Sandy silt (Unit I)
Silty sand (Unit II)
Diatom-rich sandy silt
Diatom-rich silty sand
Gravel-rich

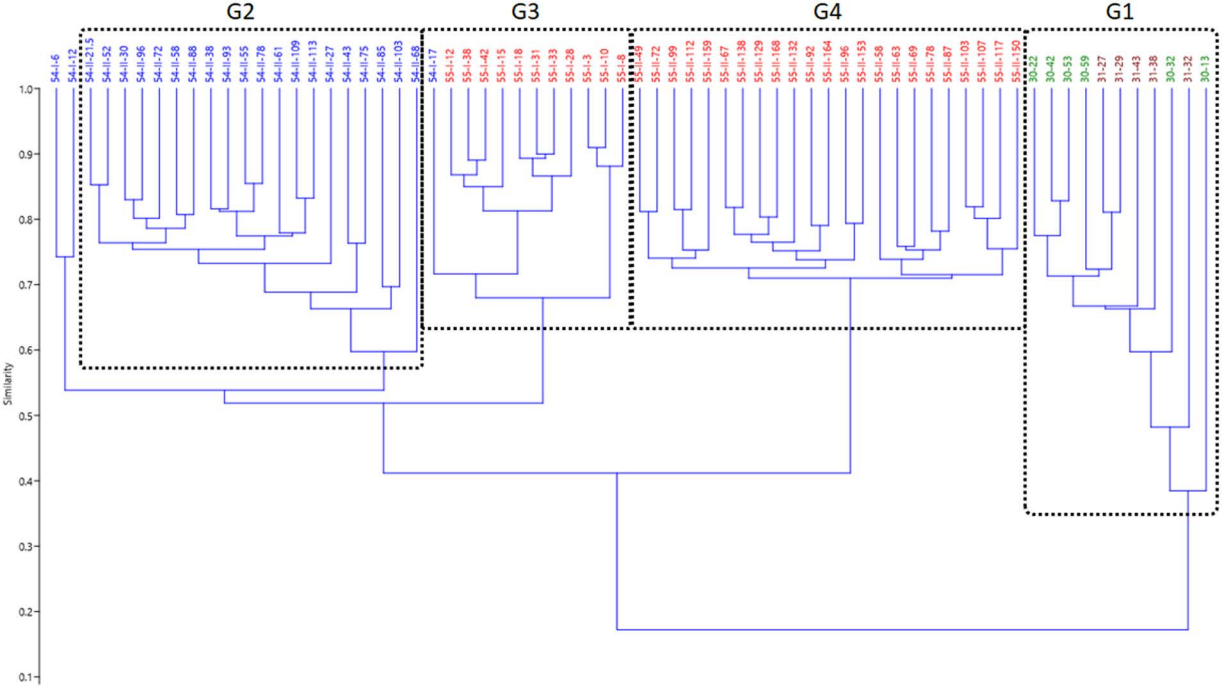
G2
G3
G4
G1
Similarity
1.0
0.9
0.8
0.7
0.6
0.5
0.4
0.3
0.2
0.1
54-I-6
54-I-12
54-II-21.5
54-II-52
54-II-30
54-II-96
54-II-72
54-II-58
54-II-88
54-II-38
54-II-93
54-II-55
54-II-78
54-II-61
54-II-109
54-II-113
54-II-27
54-II-43
54-II-75
54-II-85
54-II-103
54-II-68
55-I-17
55-I-12
55-I-38
55-I-42
55-I-15
55-I-18
55-I-31
55-I-33
55-I-28
55-I-3
55-I-10
55-I-8
55-II-159
55-II-72
55-II-99
55-II-112
55-II-159
55-II-67
55-II-138
55-II-129
55-II-168
55-II-132
55-II-92
55-II-164
55-II-96
55-II-153
55-II-58
55-II-63
55-II-69
55-II-78
55-II-87
55-II-103
55-II-107
55-II-117
55-II-150
30-22
30-42
30-53
30-59
31-27
31-29
31-43
31-38
30-32
31-32
30-13

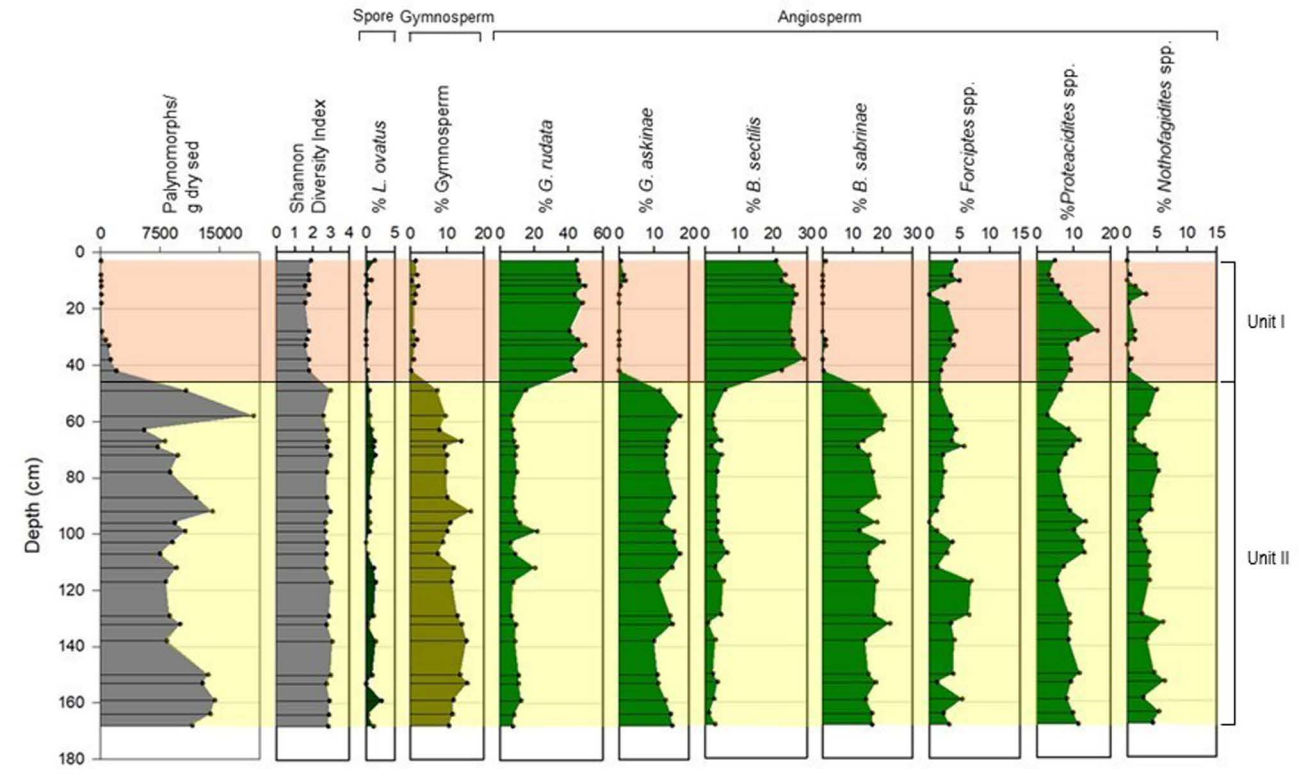
Spore
Gymnosperm
Angiosperm
Palynomorphs/ g dry sed
Shannon Diversity Index
% L. ovatus
% Gymnosperm
% G. rudata
% G. askinae
% B. sectilis
% B. sabrinae
% Forciptes spp.
%Proteacidites spp.
% Nothofagidites spp.
0 7500 15000
0 1 2 3 4
0 5
0 10 20
0 20 40 60
0 10 20
0 10 20 30
0 10 20 30
0 5 10 15
0 10 20
0 5 10 15
Depth (cm)
0 20 40 60 80 100 120 140 160 180
Unit I
Unit II

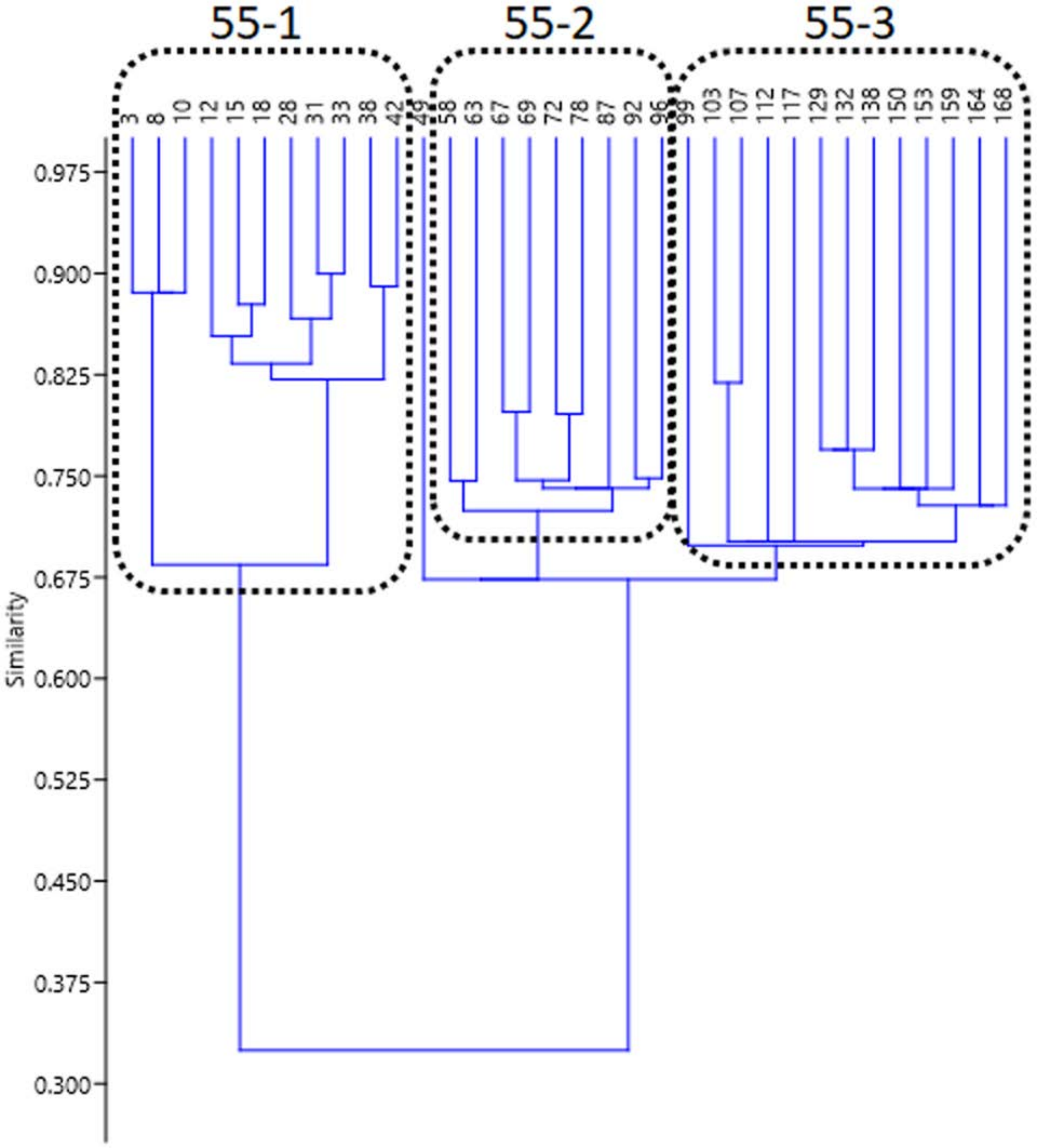
55-1
55-2
55-3
3
8
10
12
15
18
28
31
33
38
42
49
58
63
67
69
72
78
87
92
96
99
103
107
112
117
129
132
138
150
153
159
164
168
0.975
0.900
0.825
0.750
0.675
0.600
0.525
0.450
0.375
0.300
Similarity

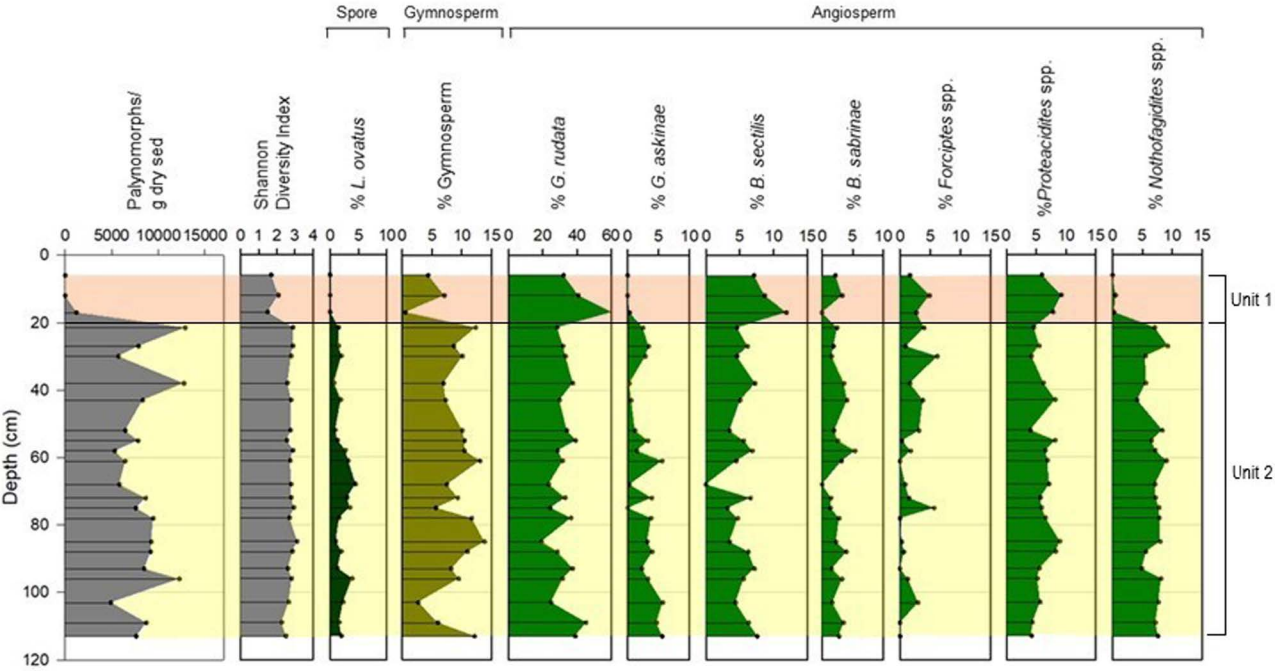
Spore
Gymnosperm
Angiosperm
Palynomorphs/ g dry sed
Shannon Diversity Index
% L. ovatus
% Gymnosperm
% G. rudata
% G. askinae
% B. sectilis
% B. sabrinae
% Forciptes spp.
%Proteacidites spp.
% Nothofagidites spp.
0 5000 10000 15000
0 1 2 3 4
0 5 10 0
0 5 10 15 0
0 20 40 60 0
0 5 10 0
0 5 10 15 0
0 5 10 0
0 5 10 15 0
0 5 10 15 0
0 5 10 15
Depth (cm)
0
20
40
60
80
100
120
Unit 1
Unit 2

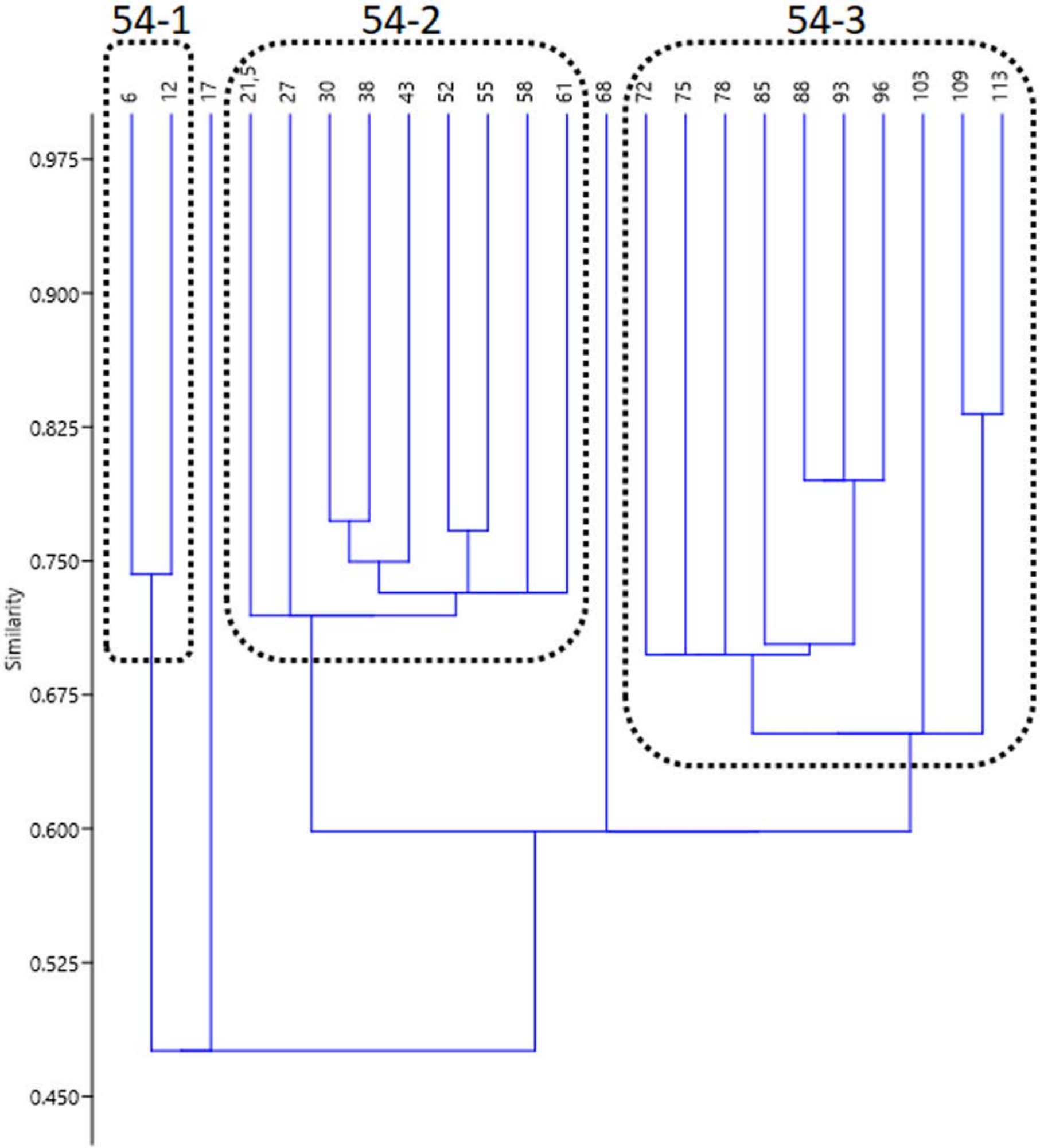
54-1
54-2
54-3
6
12
17
21,5
27
30
38
43
52
55
58
61
68
72
75
78
85
88
93
96
103
109
113
0.975
0.900
0.825
0.750
0.675
0.600
0.525
0.450
Similarity

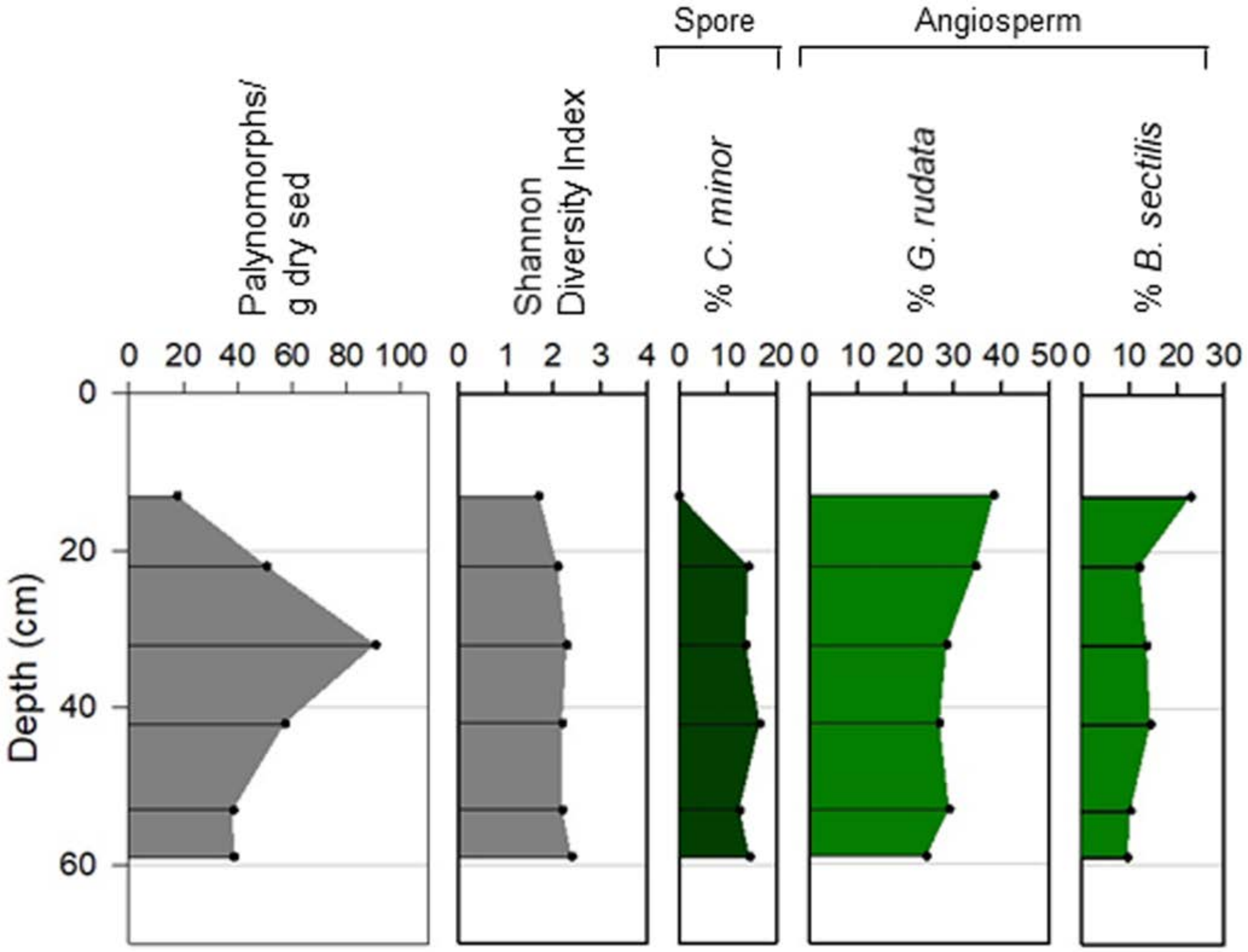
Spore
Angiosperm
Palynomorphs/ g dry sed
Shannon Diversity Index
% C. minor
% G. rudata
% B. sectilis
0 20 40 60 80 100
0 1 2 3 4
0 10 20
0 10 20 30 40 50
0 10 20 30
Depth (cm)
0
20
40
60

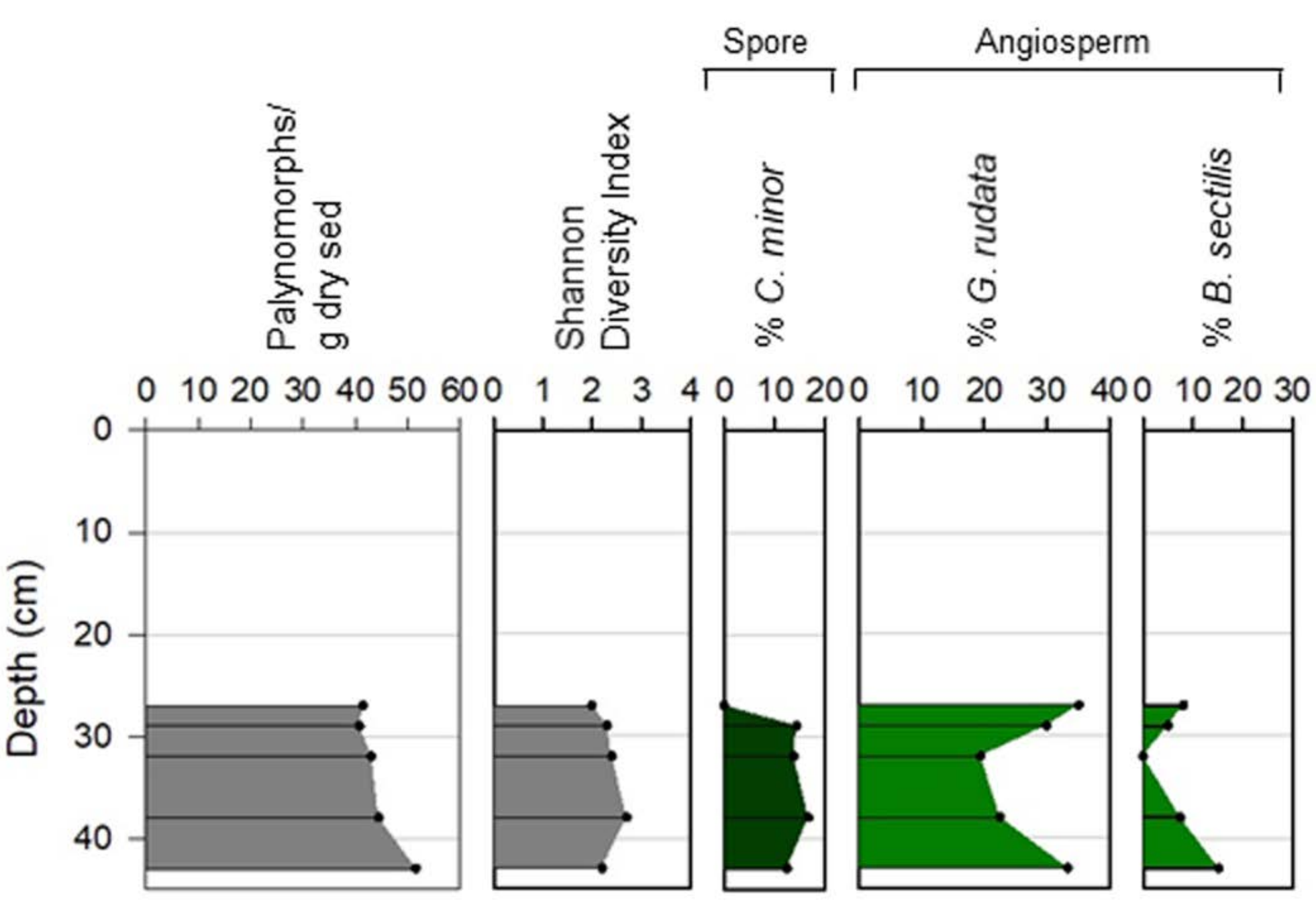
Spore
Angiosperm
Palynomorphs/
g dry sed
Shannon
Diversity Index
% C. minor
% G. rudata
% B. sectilis
0 10 20 30 40 50 60
0 1 2 3 4
0 10 20
0 10 20 30 40
0 10 20 30
Depth (cm)
0
10
20
30
40

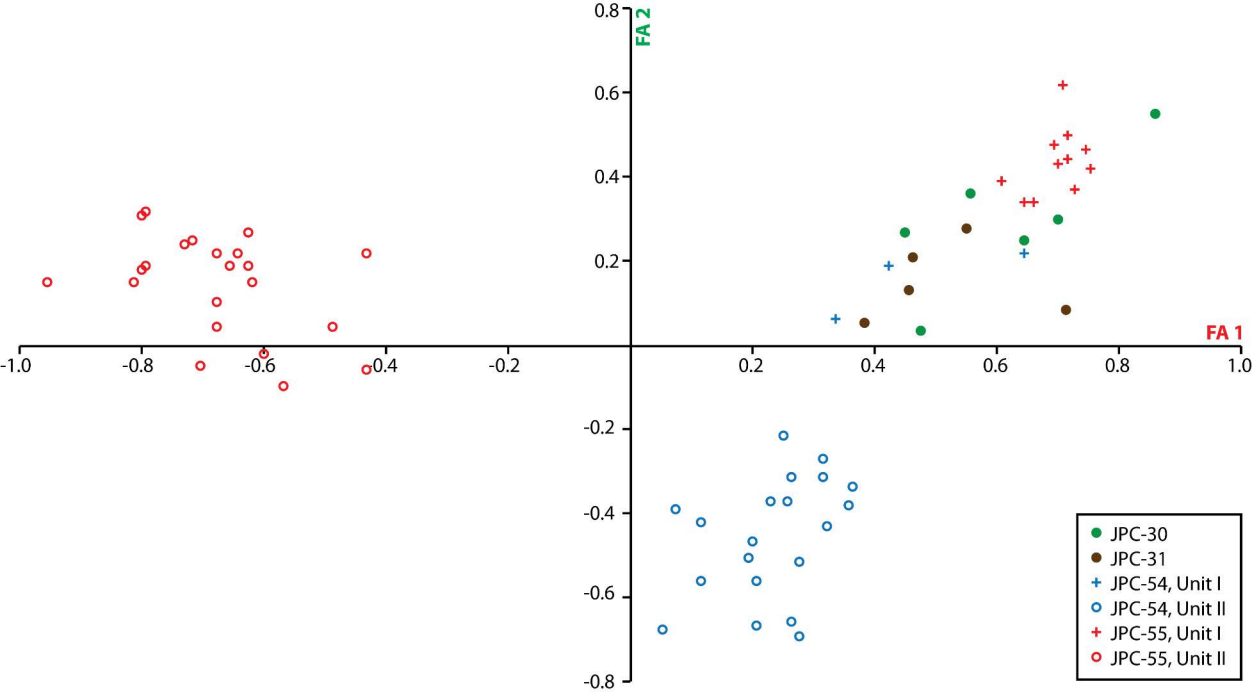
FA 2
FA 1
0.8
0.6
0.4
0.2
-0.2
-0.4
-0.6
-0.8
-1.0
-0.8
-0.6
-0.4
-0.2
0.2
0.4
0.6
0.8
1.0
JPC-30
JPC-31
JPC-54, Unit I
JPC-54, Unit II
JPC-55, Unit I
JPC-55, Unit II

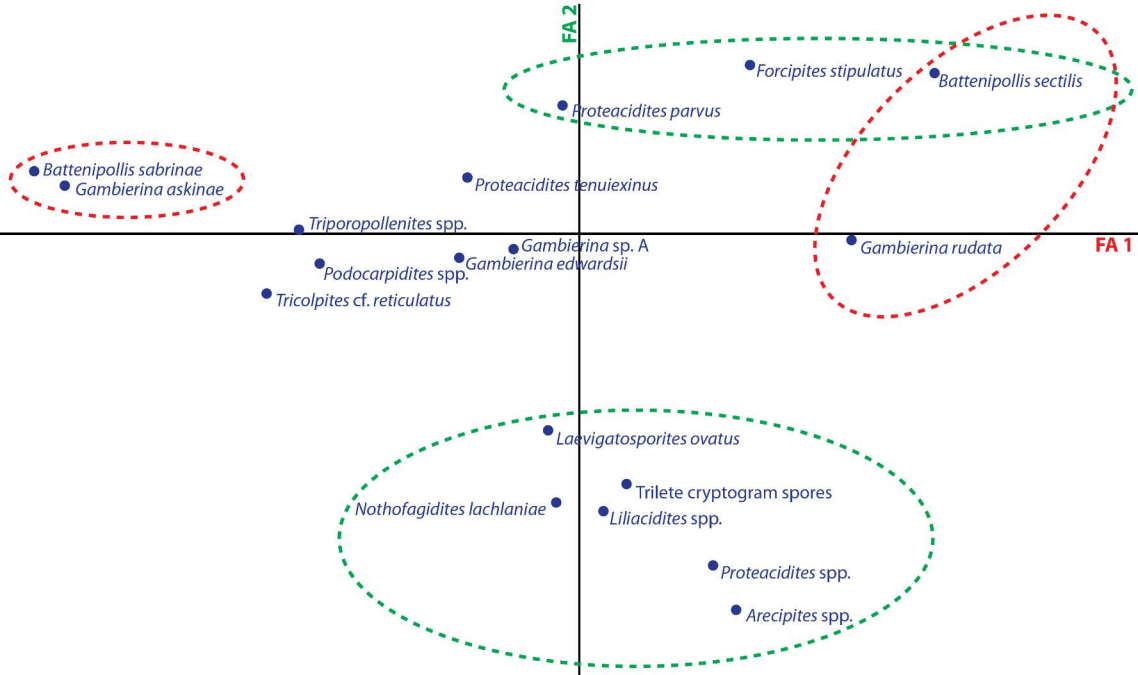
FA 2
FA 1
Forcipites stipulatus
Battenipollis sectilis
Proteacidites parvus
Battenipollis sabrinae
Gambierina askinae
Proteacidites tenuiexinus
Triporopollenites spp.
Gambierina sp. A
Gambierina rudata
Gambierina edwardsii
Podocarpidites spp.
Tricolpites cf. reticulatus
Laevigatosporites ovatus
Trilete cryptogram spores
Nothofagidites lachlaniae
Liliacidites spp.
Proteacidites spp.
Arecipites spp.

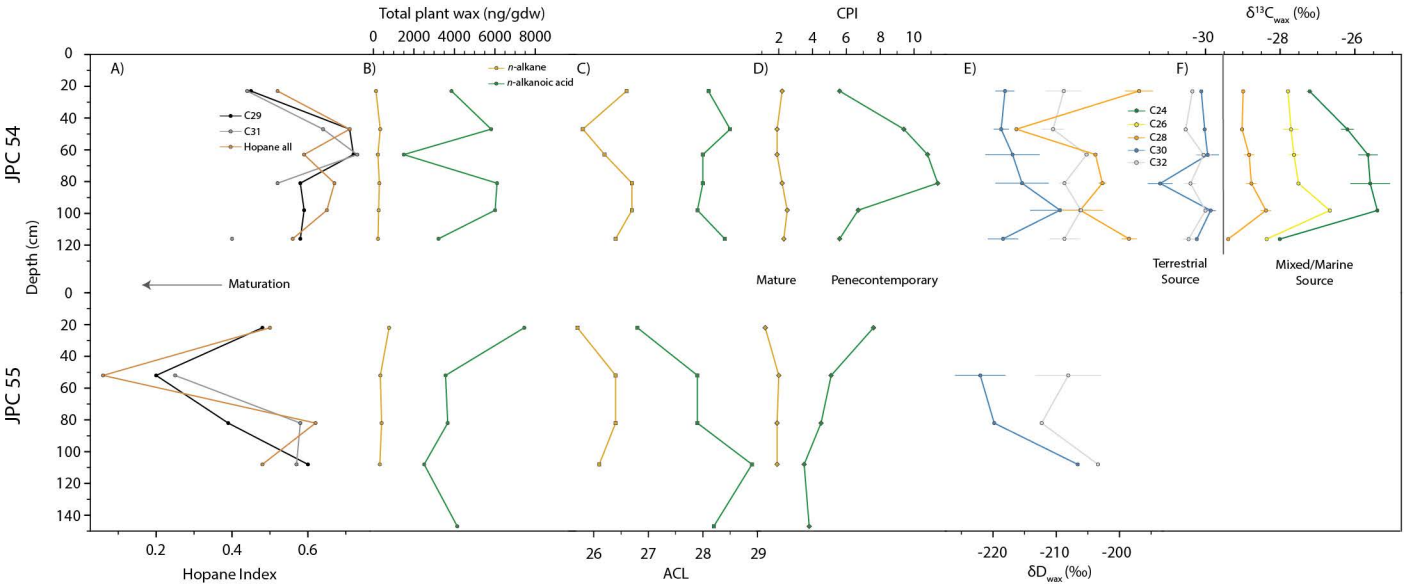
Total plant wax (ng/gdw)
0 2000 4000 6000 8000
CPI
2 4 6 8 10
δ13Cwax (‰)
-30 -28 -26
A)
B)
C)
D)
E)
F)
C29
C31
Hopane all
n-alkane
n-alkanoic acid
C24
C26
C28
C30
C32
JPC 54
JPC 55
Depth (cm)
Maturation
Mature
Penecontemporary
Terrestrial Source
Mixed/Marine Source
0.2 0.4 0.6
Hopane Index
26 27 28 29
ACL
-220 -210 -200
δDwax (‰)

Table 1.

	Taxon	Average dissimilarity	% Contribution	% Cumulative	Mean G1	Mean G2	Mean G3	Mean G4
Taxa A	*Gambierina rudata*	15.29	23.00	23.00	12.3	109.00	137.00	33.00
	Battenipollis sabrinae	6.61	9.94	32.94	0.00	7.95	1.00	52.60
	Battenipollis sectilis	6.01	9.04	41.98	4.55	18.00	76.40	11.40
	Gambierina askinae	5.65	8.49	50.48	0.00	9.00	0.82	44.60
Taxa B	*Gambierina edwardsii*	3.24	4.87	55.34	0.73	19.70	15.10	23.60
	Podocarpidites spp.	2.66	4.01	59.35	1.82	13.20	3.73	21.30
	Proteacidites parvus	2.50	3.76	63.11	1.55	6.71	21.70	15.30
	Nothofagidites lachlaniae	1.85	2.79	65.89	0.00	14.30	0.09	5.43
	Liliacidites spp.	1.18	1.78	67.67	0.00	9.10	0.00	2.83
Taxa C	*Triporopollenites* spp.	1.11	1.68	69.35	0.18	3.95	2.36	7.96
	Gambierina sp. A	1.08	1.63	70.98	0.09	6.14	5.36	6.17
	Trilete cryptogram spores	1.05	1.57	72.55	0.55	8.29	1.18	2.61
	Proteacidites spp.	1.02	1.54	74.09	0.00	8.43	0.00	0.96
	Proteacidites tenuiexinus	0.89	1.33	75.42	1.09	4.05	3.18	6.17
	Tricolpites reticulatus cf	0.87	1.31	76.73	0.18	3.76	0.273	5.61
	Arecipites spp.	0.83	1.15	77.98	0.09	6.81	0.18	0.74
	Laevigatosporites ovatus	0.83	1.24	79.22	0.64	6.62	0.73	3.13
	Forcipites sp. C	0.82	1.23	80.45	0.73	2.00	7.27	2.61